PHOTOLUMINESCENCE STUDIES OF THERMAL DONORS IN SILICON

by

Yubo Yang

B.Sc., Peking University, 1987

THESIS SUBMITTED IN PARTIAL FULFILLMENT OF
THE REQUIREMENTS FOR THE DEGREE OF
Master of Science
in the Department
of
Physics

SIMON FRASER UNIVERSITY

July 1995

APPROVAL

Name: Yubo Yang

Degree: Master of Science

Title of thesis: Photoluminescence Studies of Thermal Donors in Si

Examining Committee:

Chair: Dr. John Bechhoefer

Dr. Mike L.W. Thewalt
Senior Supervisor

Dr. Jeffrey R. Dahn

Dr. Simon P. Watkins

Dr. Barbara J. Frisken
Internal Examiner

Date Approved: July 28, 1995

PARTIAL COPYRIGHT LICENSE

I hereby grant to Simon Fraser University the right to lend my thesis, project or extended essay (the title of which is shown below) to users of the Simon Fraser University Library, and to make partial or single copies only for such users or in response to a request from the library of any other university, or other educational institution, on its own behalf or for one of its users. I further agree that permission for multiple copying of this work for scholarly purposes may be granted by me or the Dean of Graduate Studies. It is understood that copying or publication of this work for financial gain shall not be allowed without my written permission.

Title of Thesis/Project/Extended Essay

Photoluminescence Studies of Thermal Donors in Silicon

Author: _____
(signature)

Yubo Yang
(name)

Aug 11, 1995
(date)

ABSTRACT

The series of thermal donors in oxygen-doped float zone silicon has been studied in great detail here for the first time using Fourier transform photoluminescence spectroscopy. The dependence of the thermal donor bound exciton luminescence intensities on both annealing time and measurement temperature has been investigated.

More than 40 thermal donor bound exciton photoluminescence transitions have been clearly resolved at a temperature of 1.24 Kelvin. Both thermal donor ground states and valley orbit excited states play significant roles in thermal donor bound exciton luminescence. Four transitions, which are from the same initial exciton states localized on the same thermal donor species, have been conclusively identified, and the valley orbit splittings of this thermal donor species has been measured directly for the first time. The exciton binding energies of the thermal donors range from 0.50 to 8.04 meV, which is much smaller than the previously reported values. It is found that the earlier a thermal donor species is introduced into the silicon crystal during thermal annealing, the deeper its donor ground state is, while the shallower its bound exciton becomes.

ACKNOWLEDGMENTS

It has been a great honor and privilege for me to have been supervised by Prof. Mike L.W. Thewalt during the course of this research. His guidance has taught me physics as well as a great many other things.

Special thanks to Mr. Peter Horoyski, Jinsheng Hu, Dr. Jeff Wolk, and all the members of the Thewalt lab for their help and encouragement.

Financial support from Simon Fraser University and Prof. Mike L.W. Thewalt was greatly appreciated.

TABLE OF CONTENTS

TABLE OF CONTENTS (CONTINUED)

LIST OF TABLES

LIST OF FIGURES

LIST OF ABBREVIATIONS

BE	bound exciton
BMEC	bound multiexcitonic complex
Cz	Czochralski
DLTS	deep level transient spectroscopy
EHD	electron-hole droplet
EMT	effective mass theory
FE	free exciton
FTS	Fourier transform spectroscopy
FWHM	full width half maximum
FZ	float zone
IR	infrared
LO	longitudinal optical (phonon)
NP	no-phonon
O_h	full cubic symmetry
O_i	interstitial oxygen
$[O_i]$	interstitial oxygen concentration
PL	photoluminescence
Si	silicon
TA	transverse acoustic (phonon)
T_d	tetrahedral symmetry
TD	thermal donor
TO	transverse optical (phonon)
UHP	ultrahigh purity
VOS	valley-orbit splitting

Chapter One
Excitons and Photoluminescence in Silicon

1.1 Introduction

Heat treatment of oxygen-rich carbon-lean silicon (Si) at temperatures between 350 °C to 500 °C can produce electrically active centers, which are generally called thermal donors. Thermal donors were first reported in 1954 [54F]. Thermal donors are unwanted donors in silicon. Sufficient amount of thermal donors can change the material conductivity from p-type to n-type and bring deleterious effect on silicon device performance. Since their first discovery in 1954, the study of thermal donors in silicon has been of interest to both the industrial and the scientific communities for more than forty years. Although many different kinds of experimental techniques have been used to study thermal donors, their exact chemical composition and microscopic structure still remain unclear.

In this thesis, Fourier transform spectroscopy has been applied to the study of photoluminescence (PL) from thermal donors. The results presented here represent state-of-the-art resolution and the best signal-to-noise ratio photoluminescence spectra from thermal donors in silicon to

date. New spectral features have been observed and an explanation for these will be presented in this thesis.

This chapter will discuss excitons in silicon and their photoluminescence. The discussion will include an introduction to the silicon structure, valley-orbit splitting, photoluminescence, and a brief introduction to the Shell model. Chapter Two reviews studies on thermal donors. The apparatus and experimental techniques used to perform the experiments are described in Chapter Three. Chapter Four, which is the core chapter of this thesis, presents the results from the PL studies of thermal donors and related discussions. The conclusion of this study is given in Chapter Five.

1.2 Silicon

Silicon crystallizes in a diamond structure, which consists of two interpenetrating face-centered cubic (fcc) Bravais lattices, displaced along the body diagonal of the cubic cell by one quarter the length of the diagonal. It can be regarded as a fcc lattice with a two-atom basis. The basis atoms are located at (000) and a/4(111), and the crystal lattice constant a is 5.43 Å [89L]. Figure 1.1(a) shows the silicon crystal structure. Pure silicon exhibits full cubic symmetry and belongs to the O_h point group. The first Brillouin zone for the fcc lattice is a "truncated octahedron" which is shown in Figure 1.1(b).

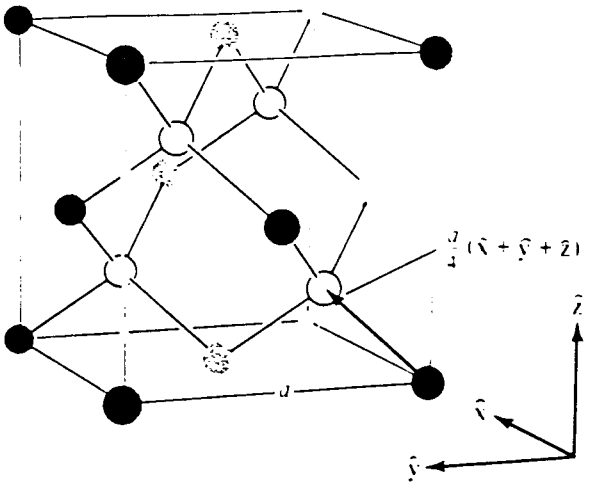

(a)

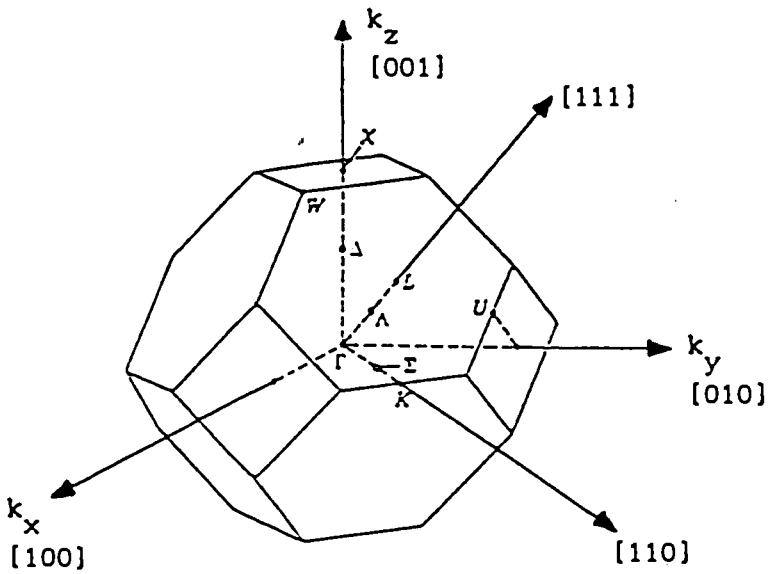

(b)

Figure 1.1 (a) Conventional cubic cell of the silicon diamond crystal structure. For clarity, sites corresponding to one of the two interpenetrating fcc cubic lattices are unshaded. Nearest-neighbor bonds have been drawn in. The four nearest neighbors of each point form the vertices of a regular tetrahedron. (b) The first Brillouin zone of the face-centered cubic lattice.

The energy band structure of silicon is depicted in Figure 1.2(a), which shows the energy of one-electron levels as a function of wavenumber along various directions in $\vec{k}$-space (reciprocal space), including the <111>, <001> and <110> directions. A conduction band minimum occurs along the <001> direction 85% of the way to the zone boundary [89L]. The constant energy surface near the bottom of this conduction band valley is an ellipsoid of revolution which has its long axes along the [001] direction. The full cubic symmetry of the lattice implies that a conduction band minimum occurs along each of the six equivalent <001> directions and thus the constant energy surfaces in $\vec{k}$-space consist of six symmetry-related equivalent ellipsoidal pockets, as depicted in Figure 1.2(b). The degeneracy of these six equivalent conduction band minima can be broken by valley-orbit splitting of the electron ground state caused by impurities, which will be discussed in Section 1.4.

The valence band maximum occurs at $\vec{k}$ = 0 (Γ point) in the first Brillouin zone, where two degenerate bands (not counting spin) with different curvatures meet, giving rise to "light holes" and "heavy holes". Note that this Si band structure has not included the spin-orbit interaction, so the valence band maximum shows three-fold degeneracy, instead of the actual two-fold degeneracy at the Γ point. The constant energy surface near the top of the valence band, which consists of two concentric warped spheres, is thus complicated [82S].

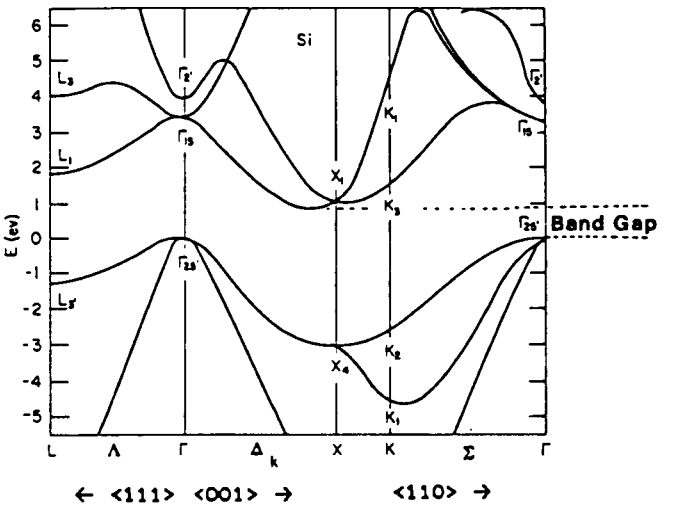

(a)

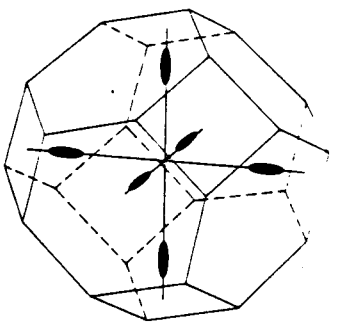

(b)

Figure 1.2 (a) Silicon band structure. (b) Constant-energy surface near the conduction band minima in silicon. There are six symmetry-related ellipsoidal pockets. The long axes are directed along <100> directions.

1.3 Impurity and Effective -Mass Theory

Donors are impurities that supply additional electrons to the conduction band, and acceptors are impurities that supply additional holes to (i.e. capture electrons from) the valence band. Effective mass theory (EMT) describes the electronic energy levels of the valence electron (or hole) of an impurity in the crystal lattice. In this theory, the ionized impurity core and its valence electrons (or holes) are treated by analogy to the hydrogen atom. The obtained energy levels relative to that of the free particles (i.e. electrons in the conduction band or holes in the valence band) are:

$$E_n = \frac{-m^* \cdot e^4}{2(h/2\pi)^2 \varepsilon^2 n^2} \qquad n = 1, 2, 3, \cdots$$

.....(1.1)

where m^* is the electron (or hole) effective mass and ε is the static dielectric constant of the host lattice. The factor ε accounts for the screening of the Coulomb attraction, and the effective mass m^* accounts for the lattice periodic potential influencing the motion of electrons (or holes), and thus essentially reflects the curvature of the conduction (or valence) band edges. In silicon the effective mass is anisotropic and the effective

mass tensor does not simply reduce to a scalar value m^*. For reasonable values of m^* and ε, the EMT ground state (n=1)binding energy E_n is 31 meV and the Bohr radius of the electron (or hole) can be 50 Å or more, and therefore the use of the semiclassical model with a single macroscopic static dielectric constant is consistent with the entire argument. Typical impurity ionization energies are in the meV range, while the ionization energies for atoms in free space are of the order of eV.

1.4 Valley-Orbit Splitting

Since the conduction band is identical at each of the six minima along <001> directions, the donor states are expected to be six-fold degenerate, without considering spin. This degeneracy can be split in the presence of impurities with chemical potentials different from pure silicon. This causes valley-orbit splitting. Valley-orbit splitting (VOS) can be understood by constructing wave functions which conform to the local symmetry of the impurity in silicon [55K,75B,81L,81R]. When a substitutional impurity is introduced to a pure silicon crystal, it takes the place of a silicon atom in the lattice, and the local symmetry in the vicinity of the impurity is reduced from the full cubic O_h symmetry to tetrahedral T_d symmetry. The resulting wave functions can be shown to be basis functions for the irreducible representations $\Gamma_1 + \Gamma_3 + \Gamma_5$ in the T_d

point group. Therefore, the donor 1s ground state is valley-orbit split into a singlet $1s\{\Gamma_1\}$, a doublet $1s\{\Gamma_3\}$, and a triplet $1s\{\Gamma_5\}$. In silicon the $1s\{\Gamma_1\}$ state is typically the lowest in energy. Electrons in the electronic excited states such as 2s, 2p ... have a low probability of coming close to the impurity site, particularly for those in odd parity states, thus the valley-orbit splitting of these states can be neglected.

If the local symmetry of a donor is lower than T_d symmetry, the electron valley-orbit states $1s\{\Gamma_3\}$ and $1s\{\Gamma_5\}$ can be further split. For example, if the donor's local symmetry belongs to the C_{2v} point group, the valley-orbit $1s\{\Gamma_3\}$ state can be split into two singlet states, and the $1s\{\Gamma_5\}$ state can be split into three singlet states.

1.5 Excitons

An exciton is an electron-hole pair bound by the electrostatic interaction. It is typically formed when a photon with energy larger than the band-gap energy excites an electron from the valence band to the conduction band, leaving a hole in the valence band. At low temperature the electron and hole can bind together via the Coulomb force to form a free exciton (FE), or in the presence of impurities, bound exciton (BE). The free excitons are free to move through the crystal, while the bound excitons are spatially localized to the impurities.

In semiconductors the exciton can be treated by analogy to the hydrogen atom, as was done for neutral impurities in Section 1.3. Therefore, the energy levels of exciton are:

$$E_b^n = \frac{\mu \cdot e^4}{2\,(h/2\pi)^2 \varepsilon^2 n^2} \qquad n = 1, 2, 3, \cdots \qquad \text{.....(1.2)}$$

where μ is a reduced mass given by $\mu \equiv (1/m_e^* + 1/m_h^*)^{-1}$. Choosing typical μ and ε values for silicon -- μ equal to 0.12 m_o (m_o being the free space electron mass) [77R] and ε equal to 12.1, Equation 1.2 yields a binding energy associated with lowest energy state of the free exciton of about 11 meV, and a "Bohr radius" of approximately 53 Å, compared to the hydrogen atom binding energy of 13.6 eV and Bohr radius of 0.51 Å. The low binding energy of exciton (~11 meV) shows that the exciton can only exist at cryogenic temperature. These extended free excitons with "Bohr radius" much larger than the lattice constant are known as Wannier-Mott excitons, which were first proposed by Wannier in 1937 [37W].

A free exciton traveling in a crystal can become localized at an impurity site, thus forming a complex called a bound exciton (BE). The existence of bound excitons was first proposed by Lampert [58L] and later observed experimentally by Haynes [60H] who noted sharp lines in the photoluminescence of silicon at energies lower than the free exciton energy. These lines are sharp because the BEs are localized at impurity sites, so that broadening of the

energy spectrum due to Maxwell-Boltzmann distribution in kinetic energies, which is typical for the FE that moves through the crystal lattice, is absent for BEs. The energy difference between the BE and a zero kinetic energy FE is known as the BE binding energy (E_{BX}). It is this binding energy that is of interest in characterizing Si, since it is usually unique to a particular impurity.

Differences in BE binding energy for different impurities are a consequence of associated strain fields and valence charge redistribution arising from the presence of the impurity ion core. These effects are usually treated as a perturbation in the effective mass theory, known as the central cell correction. For impurity states dominated by a long-range Coulomb attraction, the central cell corrections often lead to a linear relationship between exciton binding energy E_{BX} and impurity ionization energy E_i known as Hayne's rule:

$$E_{BX} = a + b\, E_i \qquad .....(1.3)$$

This is valid to some extent in most semiconductors, with constants a and b varying among different materials [79D]. Haynes [60H] observed that $a \sim 0$ and $b \sim 0.1$ for silicon.

Dean [73D] and Baldereschi [76B] explained Hayne's rule by using first order perturbation theory. They introduced a central cell potential V_C and assumed a linear dependence of the binding energy on V_C:

$$E_i = (E_i)_{EMT} + V_c\rho_c$$
$$E_{BX} = (E_{BX})_{EMT} + V_c\delta\rho_c$$

.....(1.4)

where the subscript EMT refers to the effective mass binding energy obtained with zero central cell correction, ρ_c denotes the electronic charge in the central cell and $\delta\rho_c$ is the increased charge due to the bound exciton. The equations are combined to give:

$$E_{BX} = \left[(E_{BX})_{EMT} - (E_i)_{EMT}\frac{\delta\rho_c}{\rho_c}\right] + \frac{\delta\rho_c}{\rho_c}E_i$$

.....(1.5)

If the charge ratio $\delta\rho_c/\rho_c$ is constant for a given electron-hole mass ratio, Equation (1.5) takes the form of (1.3):

$$a = (E_i)_{EMT}\left[\left(\frac{E_{BX}}{E_i}\right)_{EMT} - \frac{\delta\rho_c}{\rho_c}\right] \quad \text{and} \quad b = \frac{\delta\rho_c}{\rho_c}$$

.....(1.6)

It is also possible that more than one exciton is bound to an impurity forming what is known as a bound multiexciton complex (BMEC) [82T]. The existence of these complexes was first proposed by Kaminiskii and Pokrovskii [70K], followed by several years of heated debate [73S,74K,76M,76D,77T]. Finally, in 1977 the debate was settled with the introduction of the Kirczenow Shell model for BEs and BMECs

[77K], which was able to explain all the experimental results known at that time [77T1, 77T2].

In the Shell model, the wave function of the BMEC is represented by the properly antisymmetrized product of single particle wave functions classified according to their transformation properties under the symmetry of the impurity, which is tetrahedral (Td) for most impurities in Si. The lowest hole shell is taken to have the four-fold degeneracy (counting spin) of the valence band edge, labeled Γ_8. As in isolated donors, the twelve-fold degeneracy of the conduction band minima (counting spin) is lifted by valley-orbit splitting to give Γ_1, Γ_3 and Γ_5 valley-orbit states. In the Shell model, it is assumed that the ordering of the valley-orbit electron states in donor complexes is the same as the ordering of the states in the corresponding isolated donors. In the original Shell model, since the Γ_3-Γ_5 splitting is much smaller than that between Γ_1 and Γ_5 in the neutral donor, the Γ_3 and Γ_5 states were combined into a single electron shell labeled as $\Gamma_{3,5}$.

The Shell model has been used to explain energy levels seen in both unperturbed silicon samples and samples under uniaxial stress or magnetic field, as well as trends in transition intensities [82T].

1.6 Photoluminescence

Photoluminescence is the radiation emitted following excitation to a nonequilibrium state cause by absorption of energy in the form of light. In a semiconductor, excitation with energy larger than the band gap creates electron-hole pairs, which quickly thermalise to the band edges by emitting phonons. At cryogenic temperatures, the electrons and holes can bind together to form FEs, or in the presence of impurities, BEs. Lifetimes of excitons in Si ranges from milliseconds to nanoseconds [86S]. The exciton electron and hole then recombine, sometimes emitting a characteristic photon, which is observed as the principal BE ($h\nu_{BE}$) or FE ($h\nu_{FE}$) line in PL spectra.

In an indirect gap semiconductor, electron-hole recombination must in general be accompanied by emission of a momentum-conserving phonon. The emitted photon is therefore shifted down in energy by the amount required for the phonon creation ($h\nu_{ph}$):

$$h\nu_{FE} = E_g - E_{FE} - h\nu_{ph}, \text{ or}$$
$$h\nu_{BE} = E_g - E_{FE} - E_{BX} - h\nu_{ph}, \qquad \text{.....(1.7)}$$

where $h\nu_{FE}$ ($h\nu_{BE}$) refers to the emission energy of a free exciton (bound exciton) with zero kinetic energy, E_g is the host band gap, E_{FE} is the electron-hole pair binding energy, and E_{BX} is the exciton binding energy. However, in doped

silicon, it is possible to see no-phonon as well as phonon-assisted transitions since spatial localization of an exciton to an impurity site in real space leads to a greater diffusion of the electron and hole wave functions in k-space. This allows greater overlap of electron and hole wave functions in k-space and thus permits electron-hole transitions which conserve k-vector without phonon participation. The intensity of no-phonon transitions will therefore increase with increasing exciton localization energy (greater localization in real space implies greater diffusion in k-space). Phonon-assisted transitions will in general be broader than no-phonon transitions because of the phonon-lifetime broadening and the dispersion in the phonon spectrum. This broadening mechanism is known as phonon-broadening and is discussed in Reference 63K.

Although PL was traditionally used only to identify impurities by measuring their bound exciton recombination energies, several authors [78T, 82K, 87M] have applied it for determining absolute impurity concentrations. The intensity ratio of the luminescence emitted by the BEs and FEs was found to be remarkably linear with the impurity concentrations in Si samples at 4.2K [82K]. McL Colley and Lightowlers [87M] published calibration curves based on the ratios of the BE to FE line intensities for B, P and Al concentrations from 10^{12} to 10^{16} cm^{-3}. Since the sample is bathed in above-band gap light at cryogenic temperature, and all the donors and acceptors are therefore neutral during

the photoluminescence measurement, the concentrations of all donors and acceptors in the crystal can be measured simultaneously. Additionally, the sensitivity is also much improved compared to other methods, such as deep level transient spectroscopy (DLTS), resistivity, etc., which only look at the uncompensated fraction of the major species of impurities.

Chapter Two
Introduction to Thermal Donors

2.1 Introduction

It is generally accepted that oxygen usually exists in silicon as an electrically neutral interstitial atom. The first observation of shallow donor formation and subsequent annihilation in oxygen-rich (Czochralski-grown) silicon in the 350-500 °C temperature range was reported in 1954 [54F]. These thermally produced oxygen-related donors are generally called thermal donors (TDs).

Silicon crystals are mainly grown by two methods: float zone (FZ) and Czochralski (Cz). The flaot zone silicon usually has a low concentration of oxygen and other residual impurities such as boron, phosphorus, and aluminum. While during the Czochralski growth of silicon crystals, oxygen is introduced into the melt from the commonly used quartz crucibles. As a result, the typical concentration of oxygen in Czochralski-grown crystals reaches the solubility limit at the melting point. When cooled to a lower temperature a crucible-grown crystal represents silicon with a supersaturated oxygen solution. Typical values for the interstitial oxygen concentration, $[O_i]$, in Cz silicon are in low- to mid-10^{17} cm^{-3} range. It was found that a large initial interstitial oxygen concentration was required for

thermal donor formation in Si from the beginning of TD studies [54F].

2.2 Properties of the Thermal Donors

The first model for the thermal donors was put forward by Kaiser et al. (KFR) [57K, 58K] to explain the kinetics of the donor formation and its dependence on the initial $[O_i]$. They measured the resistivity of their samples to obtain the total TD concentration as a function of the annealing time, and observed a maximum in the conductivity upon annealing. The initial formation rate and the maximum concentration of the TDs were found to depend approximately on the fourth and third power of the oxygen concentration, respectively. These observations led KFR to propose the so-called oxygen donors as being the electrically active clusters containing four oxygen atoms.

Fuller and Logan [57F] observed a reduction in the donor concentration with increased annealing time, or with higher temperatures (> 500 °C). This phenomenon was explained in the KFR model by proposing that the addition of further oxygen atoms to the core of the electrically active clusters neutralized its electrical activity. Although successful in describing both the formation kinetics and disappearance of oxygen donors, the KFR model predicted a much lower total donor concentration than that was observed, unless an anomalously high oxygen diffusivity, which is a

factor of 10-100 times greater than the accepted value, was invoked [58K].

The thermal donors were suggested to be double donor defects which introduce two states in the silicon energy gap by Bean and Newman [72B]. Hall effect [79W], DLTS [81K], infrared (IR) absorption [79G, 79W, 83O, 83P], and formation kinetics [84W] data confirmed the presence of two states, or two donated electrons. Thermal donors can be considered as He-like effective mass centers in Si.

Infrared absorption measurements added more detail to the experimental description of the formation of the TDs obtained by simple resistivity measurements. Wruck and Gaworezewski [79W] showed that the complicated absorption spectrum of annealed oxygen-rich Si [58H,72B,75G,77H] could be interpreted as a superposition of at least four separate double donor spectra, with absorption into both the neutral donors (TD_n°) and singly ionized donors (TD_n^+) observed simultaneously. Further, they observed that the strength and number of the spectrum lines changed depending on the duration and the temperature of annealing. With the help of the knowledge about shallow donors it could be shown that these spectra are due to a superposition of the lines of different double donors whose concentrations change during annealing. They concluded that there were in fact four different TD species, not just a single donor with a complex ground state manifold.

More recently, Pajot et al. [83P] and Oeder and Wagner [83O] extended the IR investigation and showed independently that there were at least nine members of a slightly different TD family with ground state binding energies of 50-69 meV for the neutral states and 114-156 meV for the singly ionized states. Table 2.1 gives the effective mass ionization energies for all species obtained by the three groups. All the binding energies given by the OWH group were evaluated by assuming a binding energy of 3.12 meV for the 3P± states or 6.40 meV for the 2p± states (EMT) of the neutral thermal donors. The index n (n = 1 to 11) in the list labels the different TD species, with TD1 dominating at the shortest heat treatment times and having the largest binding energy.

The observed TD ground state binding energies are distinctly larger than the "hydrogenic" EMT-prediction of 31 meV obtained by scaling the ionization energy of a H-atom (13.6 eV) by the dielectric constant and the average effective mass of conduction electrons in Si. Since a neutral double thermal donor is analogous to a He-atom rather than a H-atom, it is appropriate to scale the ionization energy of He rather than that of H. A value of 56.2 meV is thus obtained for the ground state binding energies of neutral double donors [89W], which is close to the observed ground state binding energies of neutral TDs.

We can also calculate the valley-orbit splitting (VOS) of TDs from their ionization energies if we assume that the

	E°_{ion} (meV)			E^{+}_{ion} (meV)		
TD_n	WG	PCLC	OWH	WG	PCLC	OWH
1	69.5	69.1	69.2	154.9	156.3	156.3
2	67.0	66.7	66.8	143.6	144.2	149.7
3	64.7	64.4	64.6	143.6	144.2	143.8
4	62.55	62.1	62.2	137.6	138.5	138.2
5	-	60.1	60.1	-	133.1	133.0
6	-	58.0	58.0	-	128.5	128.3
7	-	56.2	56.5	-	124±1	123.6
8	-	54.3	54.5	-	121±2	119.3
9	-	52.9	53.0	-	118±3	116.0
10	-	-	51.4	-	-	-
11	-	-	49.9	-	-	-

Table 2.1: Summary of binding energies for the various neutral and singly ionized thermal donor species as measured by these groups. The binding energies were determined using 3p±- or 2p±-transitions with EMT binding energies comparing to 3p± or 2p± transitions. All E°_{ion} were obtained at 8 K. E^{+}_{ion} were obtained at 80 K (WG, [79WB]) or 8 K (PCLC [83P] and OWH [83O]&[89W]).

binding energy of the 1s $\{1\Gamma_1, 1\Gamma_3\}$ (or $\{1\Gamma_1, 1\Gamma_5\}$) state for the TDs is equal to the 1s $\{\Gamma_3\}$ ($\{\Gamma_5\}$) binding energy for phosphorus, which is known to be 33.9 (32.6) meV, very close to the EMT 1s binding energy. Here, 1s $\{1\Gamma_1, 1\Gamma_3\}$ (or $\{1\Gamma_1, 1\Gamma_5\}$) represents the thermal donor electron state in which one electron is in the Γ_1 state and the other is in Γ_3 (or Γ_5) state, and the single particle wave functions of the above state (1s $\{1\Gamma_1, 1\Gamma_3\}$ or $\{1\Gamma_1, 1\Gamma_5\}$) have 1s-like envelopes. The calculated VOS of TDs is shown in Table 2.2. TD1, the "deepest" TD, has the "biggest" VOS of 35.3 meV, while TD11, the "shallowest" TD, has the "smallest" VOS of 16.0 meV.

The clear and unambiguous identification of a family of TDs with different donor binding energies made the KFR theory [58K] less compelling and gave rise to several new models regarding the chemical composition of the TDs [83S, 84O, 85B, 85N, 86W, 88Sa, 88M]. The explanations offered so far include the assumption of a fast diffusing molecular species, an enhancement of the oxygen diffusivity, inhomogeneous O_i distribution on a microscale right from the beginning of the thermal annealing, and most recently that interstitial Si atoms might be aggregated at a core containing oxygen atoms. In all models, small aggregates of some atomic species, usually oxygen, increase in size with longer annealing time, and form the different TD species. The concentrations of different TDs reach their maximum values independently after different annealing times. The

TD_n	E°_{ion} (meV)	VOS (meV)
1	69.2	35.3
2	66.8	32.9
3	64.6	30.7
4	62.2	28.3
5	60.1	26.2
6	58.0	24.1
7	56.5	22.6
8	54.5	20.6
9	53.0	19.1
10	51.4	17.5
11	49.9	16.0

Table 2.2 The valley-orbit splitting (VOS) for the various TD species calculated from their ionization energies by assuming that the binding energy of the 1s $\{1\Gamma_1, 1\Gamma_3\}$ (or $\{1\Gamma_1, 1\Gamma_5\}$) state for the TD species equals to 33.9 meV -- the 1s $\{\Gamma_3\}$ binding energy for phosphorus. The ionization energies are taken from [89W].

existence of this maximum is considered as a proof that the TDs can become electrically inactive during isothermal annealing. The switch-off of the electrical activity of the TDs could be induced by a rearrangement of the clusters with an appropriate activation energy either at each stage of the cluster development or only beyond a certain cluster size [84O, 86W]. However, the exact chemical composition and microscopic structure of the TDs are still unclear, and none of these models will be discussed in this thesis.

By considering the effect of uniaxial stress upon the IR absorption spectrum of the TDs, Stavola, Lee et al [85S, 86Sa] obtained important information about the site symmetry and the ground state characteristics of the TDs. They showed that the ground states of TDs^0 as well as those of TDs^+ are constructed essentially from the wave functions of only one pair of conduction band minima in the frame of EMT. The EMT-like wave functions are distorted through anisotropic "central cell" effects due to the low symmetry of the TD core. This peculiar feature of the TDs is in contrast to the situation of the shallow substitutional donors like P, As, Sb, where all conduction band minima contribute to the deepest-lying ground state wave function. The TDs have a C_{2v}-point symmetry with the two-fold axis being oriented parallel to the defect's [100] crystallographic direction at the intersection of the two (110) mirror planes. The participation of only one pair of conduction band valleys

along the two-fold axis is probably due to a large uniaxial compressive stress exerted on the surrounding lattice by the TDs along their two-fold axis thus lowering the corresponding conduction band minima with respect to the other four.

The TDs are probably the most studied defects in semiconductor research [86K]. Several other experimental techniques have been used to study the TDs, including electron paramagnetic resonance (EPR) [78M, 87G], electron nuclear double resonance (ENDOR) [86M, 88M], deep level transient spectroscopy (DLTS) [81K, 86G] and Hall effect[57F, 79G]. The correlation in the behavior of the observed signal with the resistivity or IR results *versus* annealing time was used to show that the centers studied are actually the TDs. The DLTS and ENDOR measurements indicated all the TDs have C_{2v}-point symmetry, in agreement with the IR-stress results of Stavola et al [85S, 86Sa]. The ENDOR investigations of ^{17}O-enriched FZ-Si-samples also showed clearly that TD core contains oxygen atoms.

It is not trivial to correctly identify the various TD species using techniques other than IR absorption. This is well illustrated by the EPR and ENDOR results: two separate spectra, the so-called Si-NL-8 and Si-NL-10 lines, have been found to be TD-related, and a variety of possibilities regarding the exact correlation with the TDs are still being considered [78M,86M,87G,88B].

All of the discussion so far has been on the experimental investigation of the double donors themselves. Various aspects of TDs and their experimental studies have been discussed in the above. These include: the ladder of TD ionization energies, their two charge states, the nature of the effective mass ground state manifold and the structural information on the defects. In addition, good correlation between the results obtained in different measurements were also found. Review of the studies on TDs can be found in several articles [85B, 88Sb, 89W, 94B].

2.3 Photoluminescence Studies of Thermal Donors

Photoluminescence (PL) spectroscopy cannot study the bare defect centers directly, and the correlation with other experimental techniques, such as IR absorption, becomes more difficult. However, when excitons localized on the TDs recombine radiatively, transitions from the donor bound exciton system to the neutral donor may be observed, and photoluminescence may be used to investigate the excitonic system. Fortunately, it is possible to correlate PL with IR absorption through the so-called two-electron ($2e$) transitions of the BE observed in the PL spectra [67D]. In this process, the recombining BE transfers part of its energy to raise the donor electron to an excited state, instead of leaving it in the donor ground state, which is the final state of the principal transition. The emitted

photon thus has lower energy than that of the principal BE transition, and the difference equals to the energy difference between the donor ground state and the relevant excited state.

In contrast to the electric dipole allowed transitions observed in IR absorption, no parity change takes place in the 2e transitions [67D, 80M]. This is expected since the electric moment has already been changed by the electron-hole recombination. The wave function of each electron in the BE consists of a superposition of the donor ground state (1s) and excited state wave functions of the same parity (ns, nd, etc.). After BE recombination, the valence electron can be left in one of these excited states. Since 2e transitions probe the even parity excited states of impurities, this technique provides information complementary to that obtained in IR absorption.

The first identification of a PL feature with the TDs was made by Tajima et al. [79T, 80T1, 80T2] who associated a broad featureless band in their "B-type" spectrum with the radiative decay of the bound excitons(BE) localized on the TDs. Subsequently, more TD-related PL lines were reported. A major breakthrough came when the broad featureless PL band reported by Tajima et al. was further investigated in detail by Steele and Thewalt [89S]. They identified the above band as recombination of bound excitons at thermal donors in the neutral charge state (TD^0). The band was found to contain at

least 18 sharp lines, directly confirming the multispecies character of TD's.

We have conducted a detailed photoluminescence study of thermal donors in silicon using a BOMEM Fourier transform spectrometer. High-resolution PL spectra from samples with different annealing time and at measurement temperatures with good signal-to-noise ratio have been obtained. Experimental details will be discussed in the following chapters.

Chapter Three
Experimental Setup

3.1 Samples

The samples used in these experiments were supplied by the Rockwell International Science Center specifically for our thermal donor research. All the specimens were cut from an ultrahigh-purity silicon boule diffused with oxygen during the float zone (FZ) passes. During float zone passes, high-purity silicon holders were used instead of graphite ones in order to keep the carbon contamination as low as possible. These samples were found to have high interstitial oxygen and low residual impurity concentrations. The interstitial oxygen concentration of the specimens was about $1.6x10^{18}$ cm^{-3}, as determined from the room temperature infra-red (IR) absorption of the oxygen local vibration mode at 1107 cm^{-1} using method of [80T3]. Residual donor (phosphorus) and acceptor (boron and aluminum) concentrations were $[P]=1.6x10^{12}cm^{-3}$, $[B]=2.6x10^{13}cm^{-3}$ and $[Al]=3.3x10^{12}cm^{-3}$. These concentrations were determined from the ratios of impurity bound exciton no-phonon line intensities to free exciton transverse-optic (TO) phonon-assisted replica peak intensities of PL spectra at 4.2K using the calibration curves of McL Colley and Lightowlers

[87M]. The substitutional carbon concentration was lower than 10^{15} cm^{-3} as determined by other people in our group from the room temperature IR absorption band at 605 cm^{-1} using the method in [65N].

Thermal annealing was usually conducted in air at 480 °C for various time intervals, after which the specimens were heavily etched in a [HF]:[HNO_3] = 1:10 solution and cleaned with acetone and ethanol. The specimens were then mechanically polished to a mirror finish for PL studies. Some specimens received further heat treatment at 480 °C. Although an oxide layer formed on the specimen surface during these heat treatments, removing this layer by polishing with 1μm diamond paste had no noticeable effect on the PL measurements.

3.2 Resistivity Measurement Setup

A home-made collinear four-point probe was used to measure the resistivity of the samples at room temperature. Figure 3.1 shows the sketch of the four-point probe. For a sample with an arbitrary shape, the resistivity ρ is given by

$$\rho = 2\pi s F(V / I) \qquad \text{.....(3.1)}$$

where s is the probe separation and F is a correction factor that depends on the sample geometry. A piece of boron-doped

silicon with approximately the same size and thickness as our samples and with known resistivity was used to derive the factor $2\pi sF$. The current I used ranges from 10^{-5} to 10^{-3} ampere, and the voltage V is around 10^{-4} to 10^{-3} volt. Electron and hole concentrations were determined from the resistivity measurements using the data for P and B concentrations assuming that the thermal donors do not change the mobility of electrons and holes[81T].

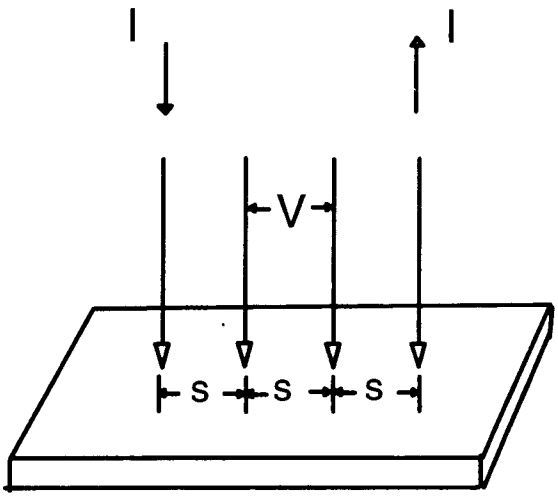

Figure 3.1 Collinear four-point probe

3.3 Photoluminescence Setup

It is useful, before going any further, to clarify the choice of units used in this thesis. In dispersive spectroscopy, the data are often collected as a function of wavelength. This is not the case in Fourier transform

spectrometer (FTS) where the spectra are usually collected as a function of wavenumber,

$$\overline{\nu} = 1/\lambda \qquad \text{.....(3.2)}$$

where λ is the wavelength of the light in vacuum. The standard unit of wavenumber is the inverse centimeter, or cm^{-1}. The photon wavenumber $\overline{\nu}$ is related to the photon frequency ν, by $\nu = c\overline{\nu}$ where c is the speed of light in vacuum. The energy in meV is related to the wavenumber by

$$E(meV) = h\ c\ \overline{\nu}(cm^{-1}) = \overline{\nu}(cm^{-1})/8.0655410 \qquad \text{.....(3.3)}$$

To allow an easy comparison of the results presented in the subsequent chapters to those reviewed above, all the spectra will be presented in meV.

A BOMEM DA8 Fourier transform spectrometer was employed to measure the PL spectra in the present study. In a Fourier transform spectrometer (FTS), spectra are collected by simultaneously sampling all wavelengths, while in a conventional dispersive spectrometer (DS), spectra are collected by sequentially measuring the wavelengths of interest.

There are two distinct advantages of a Fourier transform spectrometer over a dispersive one. The first is the so called multiplex or Fellgett advantage [86G], and arises from all the spectral wavelengths being collected

simultaneously in the FTS, in contrast to most dispersive techniques in which each resolution element is obtained separately. If the system noise is dominated by the noise of the detector, this multiplex advantage enhances the signal-to-noise ratio by a factor of $\sqrt{N}$, where N is the number of resolution elements which would be collected for the conventional dispersive spectroscopy. In the case of present study, since the thermal donor PL signal is weak, the multiplex advantage is very important, resulting in a predicted improvement in the signal-to-noise ratio over dispersive methods of approximately 10 times. The other advantage is the so called throughput or Jacquinot advantage [86G], which is due to the fact that the aperture used in an interferometer allows a much large throughput of radiation than that of a dispersive instrument, i.e. the long narrow entrance slit of a conventional dispersive instrument has a smaller area than an interferometer's circular aperture. Griffiths and de Haseth give a throughput advantage of well over 200 near 500 meV [86G].

The photoluminescence (PL) setup is described in this section. A more detailed description of the experiment setup can be found elsewhere [92N,]. Figure 3.1 shows a schematic sketch of the PL setup used in these experiments. The samples are mounted in a standard Janis immersion dewar with an optical aperture of approximately #f/3. The samples are typically immersed in boiling liquid helium (4.2K). Specimen temperatures in terms of bath temperature as low as 1.24 K

were obtained by pumping on the sample chamber with large mechanical pumps. The temperatures were determined by measuring the vapor pressure above the He liquid.

The mirror-polished surface of the specimen was irradiated by either a semiconductor diode laser (Spectra Diode Labs model SDL 800) or a Ti:Sapphire laser (Spectra-Physics model 3900) lasing near 980 nm. The laser beam was defocused to a spot size of about 5 mm in diameter on the samples. For the quenched sample, which is one of our as-received specimens briefly annealed at 1200 °C and then quenched in liquid nitrogen to break up the grown-in oxygen clusters, and short annealing-time samples, since the concentrations of thermal donors and other residual impurities were quite low in these samples, the diode laser was used to provide an excitation of about 15 mW to prevent the formation of bound multiexciton complexes (BMEC). In this case, a 1μm x 40nm bandpass filter was placed in the excitation path to block other wavelengths present in the diode laser output. For the longer annealing-time (≥ 1.0 hour) samples, because the thermal donor concentrations were quite high, the Ti:Sapphire laser was used with a higher excitation power ranging from 100 to 400 mW, which did not cause the formation of BMEC. The generation of an electron-hole liquid (EHL) was not observed. Sample heating was not serious, judging from the spectral shape of the free exciton line.

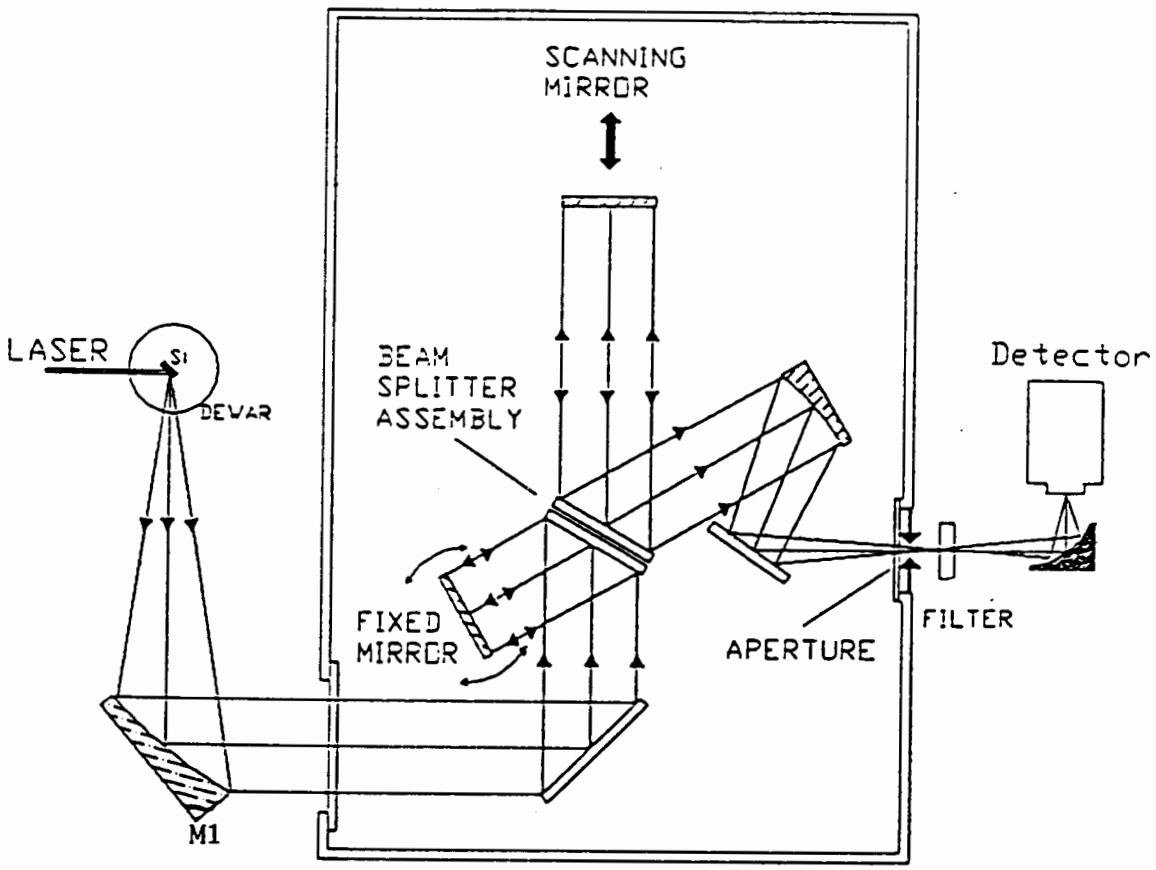

Figure 3.2 Schematic of the optical layout of the BOMEM Fourier transform PL spectroscopy set-up. The most intrinsic feature of the BOMEM is the dynamic alignment of the moving and fixed mirror, which facilitates its use at near infrared wavelengths and the collecting ultrahigh resolution spectra.

An off-axis parabolic mirror (M1) collected the photoluminescence emitted from the sample and directed it to a BOMEM DA8 Fourier transform interferometer. The PL signal coming from the sample was split by a quartz beamsplitter (B) in the FT interferometer so that the transmitted beam followed the path of a constantly moving mirror and the reflected beam was directed onto a fixed mirror. The moving and fixed mirrors reflected the signal back through the beamsplitter where the two beams recombined and interfered. The signal from the interference of the recombined beams is measured as a function of the light path difference between the two mirrors away from the beamsplitter and is called an interferogram.

There are two intrinsic characteristics of the BOMEM FT spectrometer that make it ideal for PL studies. The first is its dynamic alignment system, which operates by continually reorienting the fixed mirror to maintain alignment with the moving mirror. The dynamic alignment system employs a single mode He-Ne laser with its beam expanded and collimated into a light spot of $\cong$ 2 cm in diameter which then passes through the interferometer. After the He-Ne laser beams have recombined at the beamsplitter, an array of photo-diodes monitor the intensity across the expanded beam and servos two motors which adjust the "fixed" mirror to maintain one interference fringe over the width of the He-Ne beam. Resolution of 0.5 cm^{-1} (0.06 meV) was used throughout the work except when specified. The second characteristic is the

real-time numerical filtering, which enables very fast collection of the interferogram and subsequent calculation of the Fourier transform.

In our present studies, the interferogram was detected by either a liquid nitrogen cooled 77K Epitaxx InGaAs photovoltaic detector (model ETX 1000 TV) or a 77K fast-response North Coast Ge detector (model EO-817S). The Ge detector had a better signal-to-noise ratio in our experiment than that of the InGaAs detector. The scattered light from the excitation source, which is much more intense than the PL signal itself, was rejected by a colored glass long-pass filter (Corning 7-80) and a 990 nm holographic rejection filter placed in front of the detector. The detector output was amplified, digitized, and finally fed into a VAX 3100 M38 workstation. The Fourier transform of the interferogram was done by a vector processor on the BOMEM.

To achieve an acceptable signal-to-noise ratio, all the spectra were obtained by accumulating hundreds or thousands of scans. White light spectra with the same resolutions and at the same spectral region as the PL spectra were collected to measure the system spectral response. All the spectra were corrected for spectral response by comparing them to the white light references.

3.4 Time-resolved Photoluminescence Setup

A conventional 3/4m double grating spectrometer was used to carry out the time-resolved photoluminescence measurements. It is very difficult to do time-resolved measurements on a Fourier transform interferometer since the PL signal at all energies is recorded simultaneously as a function of the position of the moving mirror.

Figure 3.3 is the block diagram of the experimental apparatus for time-resolved photoluminescence. An acousto-optic modulator (Liconix model 50SA-0800-2000) was installed in the light path between the Ti:Sapphire laser (Spectra-Physics model 3900) and the sample to convert the continuous laser to pulsed laser. A home-built pulse generator sent a square wave signal to the acousto-optic modulator to control the laser pulse width and repetition rate. The pulsed laser had a period long enough to allow the PL signal of interest to decay between each pulse.

The luminescence from the sample, after being analyzed by a home-built double grating spectrometer, was collected by a photomultiplier tube (Varian VPM159A3) operating in the photon counting mode. A single photon can produce an output pulse large enough to be counted individually because of the high gain of the photomultiplier tube. When a photon was detected, the resulting photomultiplier current triggers the constant fraction discriminator (CFD), and a start pulse was generated and applied to the time-to-amplitude converter

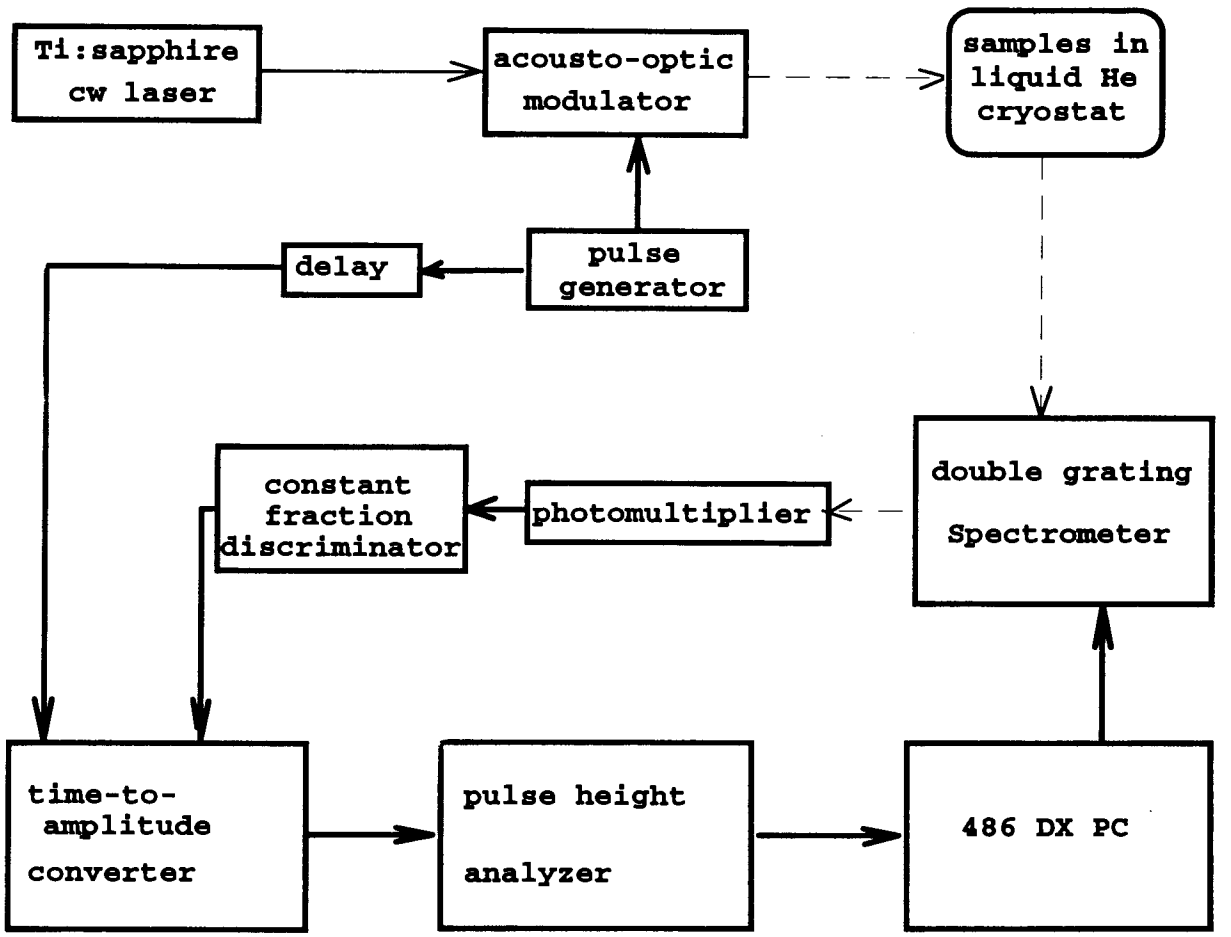

Figure 3.3 Block diagram of the experimental apparatus for time-resolved photoluminescence using a delayed coincidence photon counting system

(TAC). The stop pulses were generated by the pulse generator and were delayed so that they arrived at the TAC sometime after the start pulse. The stop rate is the same as the pulsed laser repetition rate whereas the start rate is much lower, since a luminescent photon was not always detected for every laser pulse.

When a pulse was applied to the TAC, the TAC then delivered an output pulse to the pulse-height analyzer (PHA), the amplitude of the pulse being accurately proportional to the time difference between the start and stop pulses at the TAC. The TAC output was digitized by the PHA and sent to a 486DX personal computer. The computer thus received a numerical value corresponding to the time difference between the start and stop pulses for each pair of pulses. After the collection of many such pairs, a histogram of the luminescence decay was obtained.

For the thermal donor study, the system collected a photoluminescence decay curve at each given wavelength. The pulsed laser repetition rate was 250 KHz and the laser pulse width was 0.8 μs. The TAC range was 8 μs.

Chapter Four
Results and Discussion

4.1 Resistivity Measurements

The resistivity of our quenched sample at room temperature is 1.6×10^3 Ω·cm, which corresponds to a hole concentration of 8.0×10^{12} cm^{-3}. The quenched sample was one of our as-received specimens annealed briefly at 1200°C and then quenched in liquid nitrogen to disperse the oxygen and to break up the grown-in oxygen clusters. As electrically active oxygen-related centers could have formed during the FZ silicon boule cooling from the diffusion temperature, this heat treatment is used to destroy these centers and to provide a well defined "starting" sample. The resistivity measurement result of the quenched sample is in line with the results we obtained from the PL measurements of our as-received samples.

We have converted the room-temperature resistivities to electron concentrations using the data provided in Reference 81T. Figure 4.1 is a log-log plot of the total electron concentration as a function of annealing time at 450°C. Note that the annealing temperature here is 450 °C which is lower than the other annealing temperature of 480 °C. We started with a sample annealed for five minutes at 480 °C, put it in

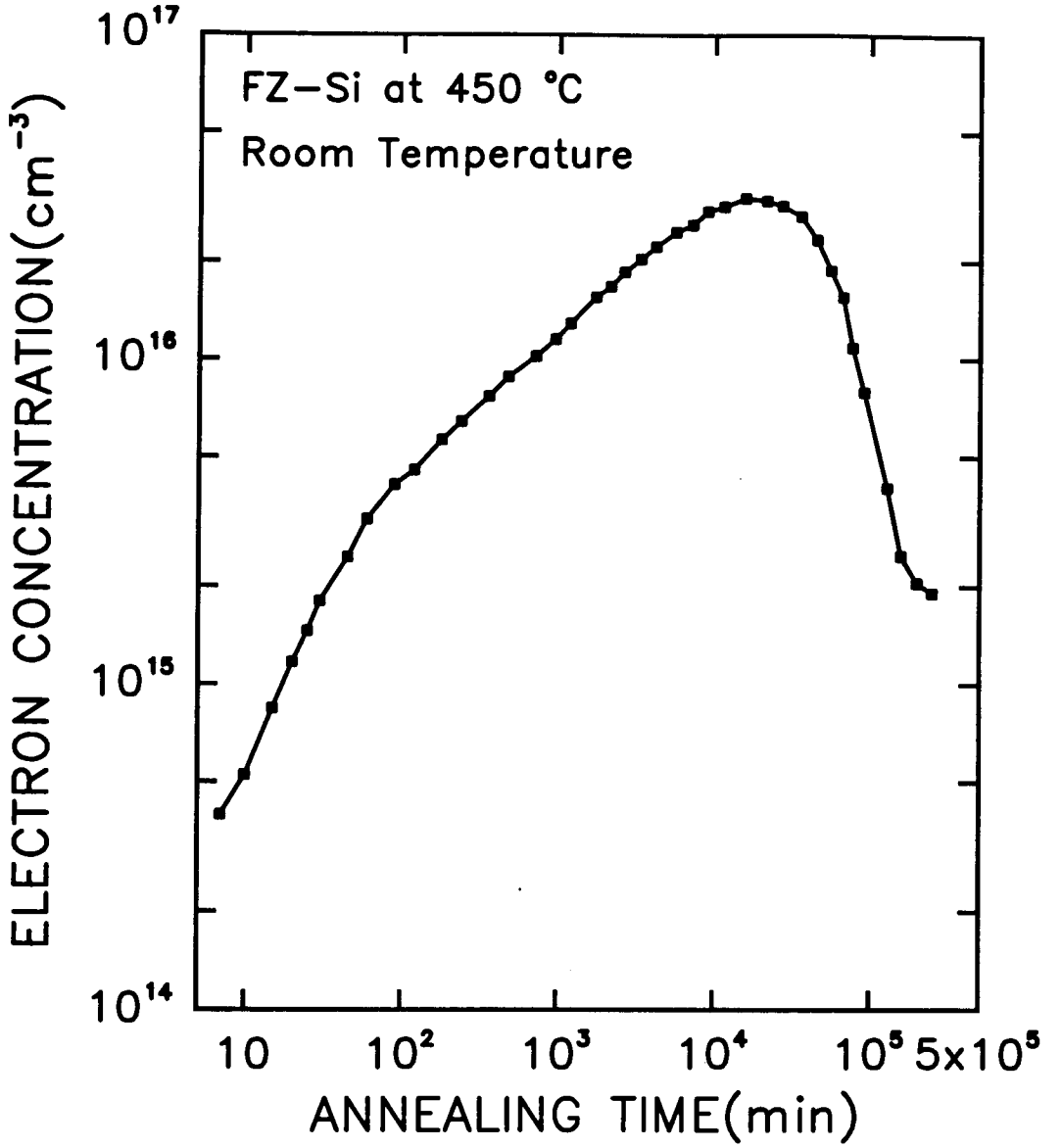

Figure 4.1 Changes of the total electron concentration with annealing time at 450 °C in air. Electron concentrations were derived from the room temperature resistivity measurements. The total thermal donor concentration is one half of the ordinate. Thermal donors have a maximum total concentration of $1.6x10^{16}$ cm^{-3} at 262 hours in this material.

the oven for some time and took out, measured its room temperature resistivity, and then put it back in the oven. This process continued till we obtained a sample with an accumulated annealing time of $2X10^5$ minutes. The total thermal donor concentration is one half of the electron concentration, if we assume that each thermal donor, which is known to be a double donor, contributes two electrons to the conduction band at room temperature. This electron concentration versus annealing time plot agrees with published data [57F, 89K]. The thermal donor concentration increases with the annealing time, reaching a maximum of $1.6x10^{16}$ cm^{-3} at 262 hours, which is two orders lower of magnitude than the interstitial oxygen concentration in our as-received samples, and then decreases with further annealing. After 4000 hours of thermal annealing, the thermal donor concentration stabilizes at around 10^{15} cm^{-3}.

The room temperature resistivity of the sample annealed for 20 minutes at 480°C is 1.5 Ω·cm. The electron concentration is $3.0x10^{15}$ cm^{-3}, and thus the TD concentration is $1.5x10^{15}$ cm^{-3}.

4.2 Photoluminescence Studies

The PL spectra from the quenched sample measured at 1.24K and a 4-hour 480 °C annealed sample measured at both 4.2K and 1.24K are shown in Figure 4.2. This figure give us

Figure 4.2 PL spectra of FZ-Si (a) quenched sample recorded at 1.24K, (b)annealed for 4 hours at 480°C, spectrum was recorded at 4.2K, (c) same sample as (b) while spectrum was recorded at 1.24K. Resolutions of all three spectra were 0.06 meV. The intensities in the NP, TA and part of the TO regions in (b) and (c) have been expanded seven times for clarity. No BMEC recombination is observed. The strongest peaks of the thermal donor NP, TA and TO bands occur at 1144.71, 1126.02, 1086.69 meV on (b) and (c). Comparing (c) with (b), new PL lines appear. S_{NP} denotes the observable no-phonon assisted decay of the shallowest TD bound excitons.

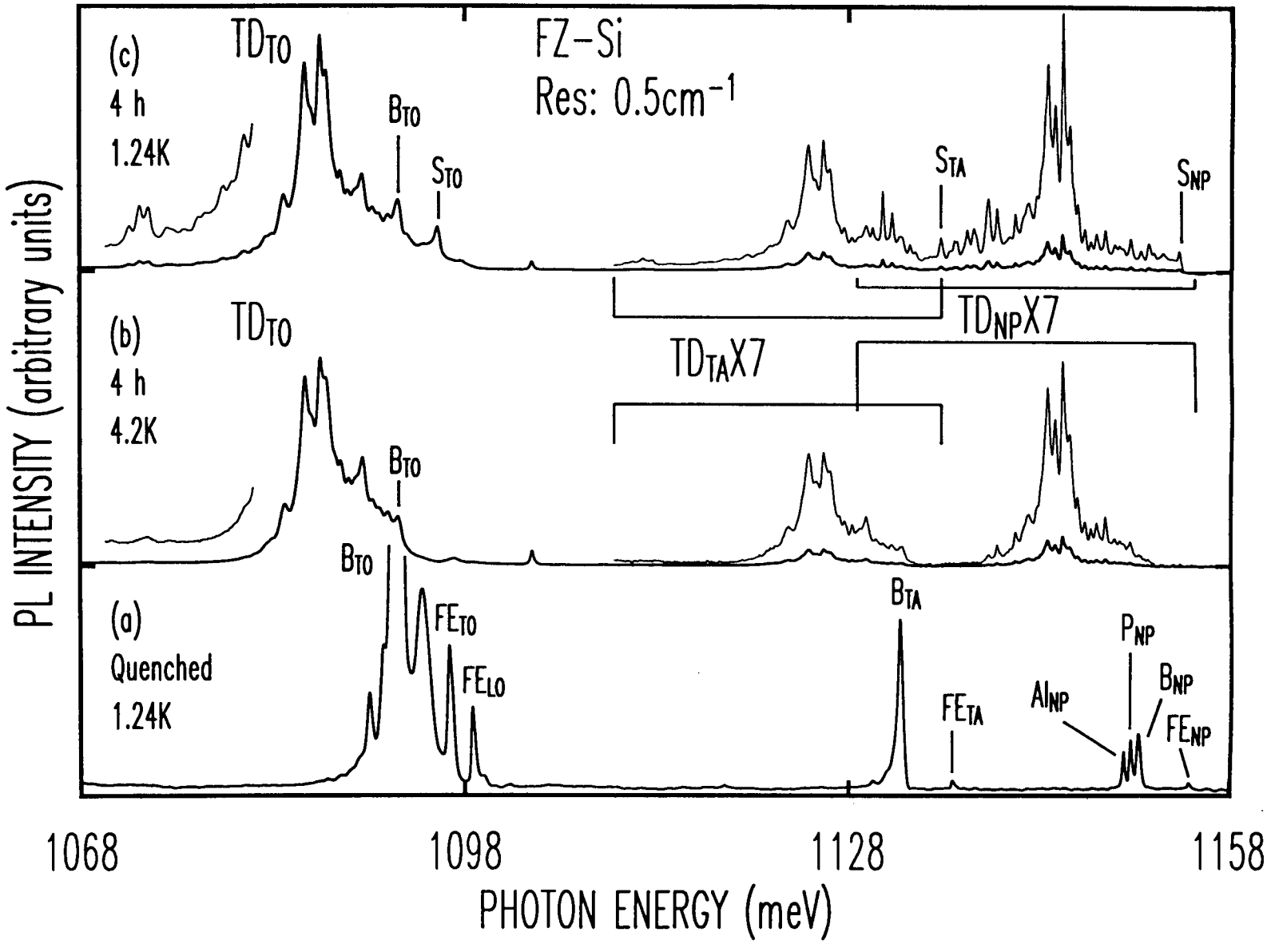
(c)
4 h
1.24K
TDTO
FZ-Si
Res: 0.5cm-1
BTO
STO
STA
SNP
(b)
4 h
4.2K
TDTO
TDTAX7
TDNPX7
BTO
(a)
Quenched
1.24K
BTO
FETO
FELO
BTA
FETA
AlNP
PNP
BNP
FENP
PL INTENSITY (arbitrary units)
1068
1098
1128
1158
PHOTON ENERGY (meV)

a general idea of what photoluminescence lines from excitons localized on thermal donors look like. The spectral pattern of Figure 4.2(a) is typical of a FZ silicon crystal with small amounts of B, P and Al impurities. In this spectrum, FE_{NP}, FE_{TA}, FE_{LO} and FE_{TO} are labels of no-phonon (NP), transverse-acoustic (TA), longitudinal-optic (LO) and transverse-optic (TO) phonon-assisted free exciton recombination peaks, respectively. The NP lines of the radiative decay of bound excitons (BEs) at neutral donors (phosphorus) and acceptors (boron and aluminum) P_{NP}, B_{NP} and Al_{NP} are clearly resolved. The TO and TA replicas of boron bound exciton recombination dominate the TO and TA region of this spectrum. No luminescence of residual donor- or acceptor-related bound multiexciton complexes (BMEC) was observed, which shows the optical excitation was at the right level. Except for the FE and B, P and Al related bound exciton recombination, there were no other PL lines in this spectrum. No thermal donors were observed in this sample.

Figure 4.2(b) is the PL spectrum from a 4-hour 480 °C annealed sample measured at 4.2K. The intensity of the NP, TA and part of TO regions has been expanded by a factor of seven for clarity. Luminescence of FE and residual impurity related BEs is very weak in this spectrum. No PL from residual impurity related BMEC was observed even though the optical excitation power is around 350 mW. The spectrum is dominated by the PL lines ascribed to bound exciton

recombination at different thermal donors by Tajima *et al.* [80T], Nakayama *et al.* [81N], Drakeford *et al.* [87D] and Steele *et al.* [89S]. Tajima *et al.* assigned the broad featureless PL band as TD_{NP}, TD_{TA}, and TD_{TO} peaked at 1.143, 1.124, and 1.085 eV, respectively [80T]. TD_{NP}, TD_{TA}, and TD_{TO} were the no-phonon, TA and TO replica of bound exciton recombination associated with the thermal donors. Drakeford *et al.* found the broad bands contain detailed structure which could be resolved. In the weak TD_{NP} band where there was no phonon broadening, Drakeford *et al.* showed that there were at least 14 sharp lines separated by ~0.5 meV and Steele *et al.* showed that there were at least 18 sharp lines. In our spectrum the fine structures of TD_{NP}, TD_{TA}, and TD_{TO} bands can be seen in great detail. These bands consist of at least 27 well resolved sharp lines. The peaks of the strongest lines in TD_{NP}, TD_{TA}, and TD_{TO} bands occur at 1144.71, 1126.02, and 1086.69 meV, respectively. Note that the peak intensity ratio of the strongest lines in the TD_{TO} to those of the TD_{NP} bands is about 7. This large TO:NP ratio will be addressed later in this section.

Figure 4.2(c) is the PL spectrum from the same 4-hour annealed sample recorded at 1.24K. Comparing with Figure 4.2(b), the main features do not change much. However, this spectrum contains some new sharp lines not present in the 4.2K spectrum. When the sample temperature is lowered, some shallower TD bound excitons form, and some thermal donors which cannot bind free excitons at 4.2K do localize free

excitons at 1.24K. S_{NP}, peaked at 1153.96 meV and with a full width at half-maximum (FWHM) of 0.22 meV, denotes no-phonon luminescence from the radiative decay of the shallowest bound exciton associated with the thermal donors. Near the B_{TA}, three new no-phonon lines become quite strong, and their replicas, a triplet structure, are clearly observed in the TO phonon assisted region.

In Figure 4.2(c) there are more than 40 separate and reproducible TD-related peaks, considerably more than the previously reported 18 peaks [88D, 89S]. Most of the peaks are quite weak compared to the strongest ones, and some peaks only appear at very low temperatures. Unfortunately, the luminescence from shallow BEs associated with the residual P, B and Al is in the energy region of the TD band. Unfortunately, it is impractical to make a Si sample with very high oxygen concentration and no residual impurities. This is because the oxygen diffusion coefficient is ten orders of magnitude lower than that of the other elements such as B, P, and Al at the diffusion temperature (~1250°C), it is impossible to prevent the contamination of the sample by B, P and Al during the oxygen diffusion process. In addition, the low energy region of the TD_{NP} band overlaps with the high energy of the TD_{TA} band. All the above factors make the TD PL spectrum extremely complicated.

Figure 4.3 is the PL spectra from the sample annealed for 20 minutes at 480 °C recorded at (a) 4.2K, (b) 2.0K, (c) 1.24K. Compared with Figure 4.2(a), the PL spectrum of the

Figure 4.3 PL spectra of FZ-Si annealed for 20 minutes at 480°C, recorded at (a) 4.2K, (b) 2.0K, (c) 1.24K. The NP, TA and part of TO regions have been enlarged 10 times. The spectra are dominated by the bound exciton emission related with boron. When the recording temperature is lowered, new TD-related PL lines become visible, which corresponds to formation of shallower TD bound excitons.

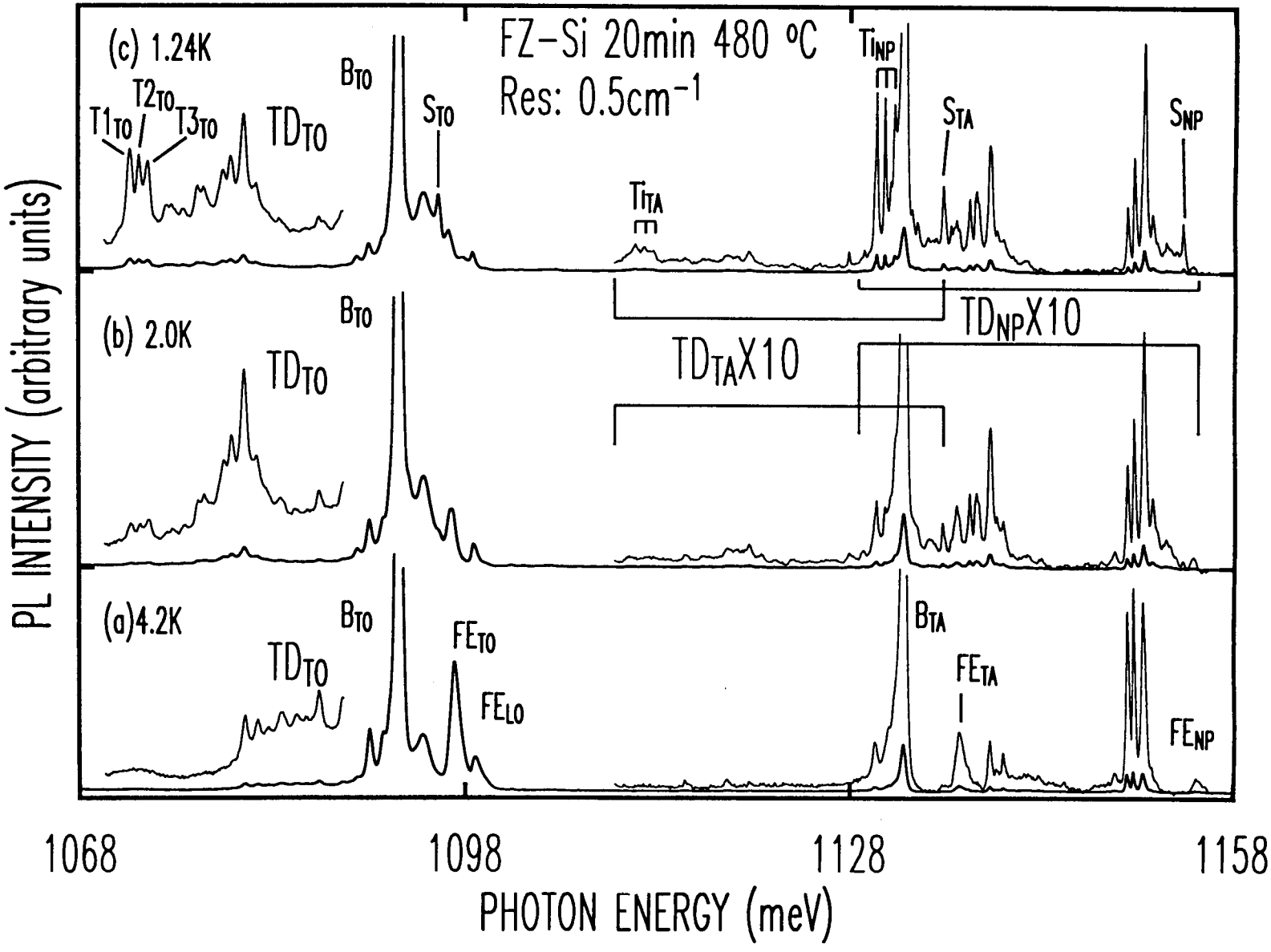
(c) 1.24K
FZ-Si 20min 480 °C
Res: 0.5cm⁻¹
T1TO
T2TO
T3TO
TDTO
BTO
STO
TITA
TINP
STA
SNP
(b) 2.0K
TDNPX10
TDTAX10
(a)4.2K
FETO
FELO
BTA
FETA
FENP
PL INTENSITY (arbitrary units)
1068
1098
1128
1158
PHOTON ENERGY (meV)

quenched sample, some new lines which are associated with thermal donors are clearly observed in Figure 4.3. However, no sign of the strongest parts of the TD bands in Figure 4.2 (b)&(c) are observed in the 20 minute sample spectra. When the temperature is lowered, the thermal activation effect is weakened and some free excitons are able to be weakly localized on specific neutral TD species. Thus the intensities of the PL from these weakly bound excitons increase when the measurement temperature is lowered.

As we have inferred from the resistivity measurement, the total TD concentration in this 20 minute sample is over 10^{15} cm^{-3}, while the residual boron concentration is just around 10^{13} cm^{-3}. The total TD concentration is two orders of magnitude higher than the boron concentration. The PL spectra of this sample is expected to be dominated by TD related decay, if the capture cross sections of excitons to the neutral TD and to the neutral boron impurity were of the same order. However, even at temperatures as low as 1.24K, the PL spectrum is still dominated by the boron bound exciton recombination. Figure 4.3 shows clearly that even at 1.24K, most of the thermal donors in this sample cannot localize any free excitons to form TD bound excitons. It is inferred from Figure 4.3 that if the temperature is lowered even further, the PL intensity from the observed shallowest TD BEs at 1.24K will increase, and the PL from some even shallower TD BEs may become observable. It is quite possible that some TD species, namely the very early ones, may not be

able to form bound excitons no matter how low the temperature is.

In Figure 4.3, we label S to be the observed shallowest TD BE transition as S, and the triplet of transitions in the TO region as $T1_{TO}$, $T2_{TO}$ and $T3_{TO}$. S_{NP}, S_{TA} and S_{TO} are the no-phonon, TA and TO phonon-assisted replicas of S, and Ti_{NP}, Ti_{TA}, and Ti_{TO} are the no-phonon, TA and TO replicas of Ti (i=1,2,3), respectively. The LO replicas of S and Ti (I=1,2,3) are so weak in our spectra that they are negligible in our analysis. It is unfortunate that $T1_{NP}$, $T2_{NP}$ and $T3_{NP}$ are in the same range of the TA replica of the decay of shallow BE associated with the residual impurities P, B and Al.

We have measured the peak intensities of the four PL lines, S_{NP}, $T1_{TO}$, $T2_{TO}$ and $T3_{TO}$, as a function of temperature. Figure 4.4 is a plot of the logarithm of the relative PL intensities of the four lines versus the reciprocal sample temperature. At low temperature,

$$I_{PL} \propto Exp(E_b / k_B \cdot T) \qquad .....(4.4)$$

where I_{PL} is PL intensity, E_b is the thermal activation energy which equals the BE binding energy, k_B is Boltzmann's constant, and T is the measurement temperature in Kelvin. The thermal activation energies, calculated from the slopes of the lines, are:

$$E_S = 0.50 \text{ meV}$$

$$E_{T1} = 0.38 \text{ meV}$$

$$E_{T2} = 0.46 \text{ meV}$$

$$E_{T3} = 0.36 \text{ meV}$$

.....(4.5)

The four TD bound exciton thermal activation energies are equal within our measurement error, which is about 0.1 meV.

In addition, we have also used Equation 1.7 to measure the binding energy E_{BX} of the shallowest TD BE (labeled S) directly from its spectral position. The photon energy of the S_{NP} line is 1153.98 meV. The photon energies of the P_{NP} and P_{TA} lines, along with the energy of the FE_{TA} edge, are precisely determined from an ultrahigh purity Si PL spectrum recorded at 1.24K with a resolution of 0.1 cm^{-1}. The P_{NP}, P_{TA} and the edge of FE_{TA} are 1150.03, 1131.38, and 1135.83 meV, respectively. The FE_{NP} edge is 1154.40 meV which is obtained by P_{NP} and P_{TA} edge energy shifted towards higher energy at the TA phonon energy. The TA phonon energy is equal to the energy difference between P_{NP} and P_{TA}, which is 18.65 meV. The bound exciton binding energy related with S transition is 0.51 meV, which is the energy difference between the S_{NP} peak and FE_{NP} edge. Thus the spectroscopically determined S-related bound exciton binding energy equals the thermal activation energy of all the four lines.

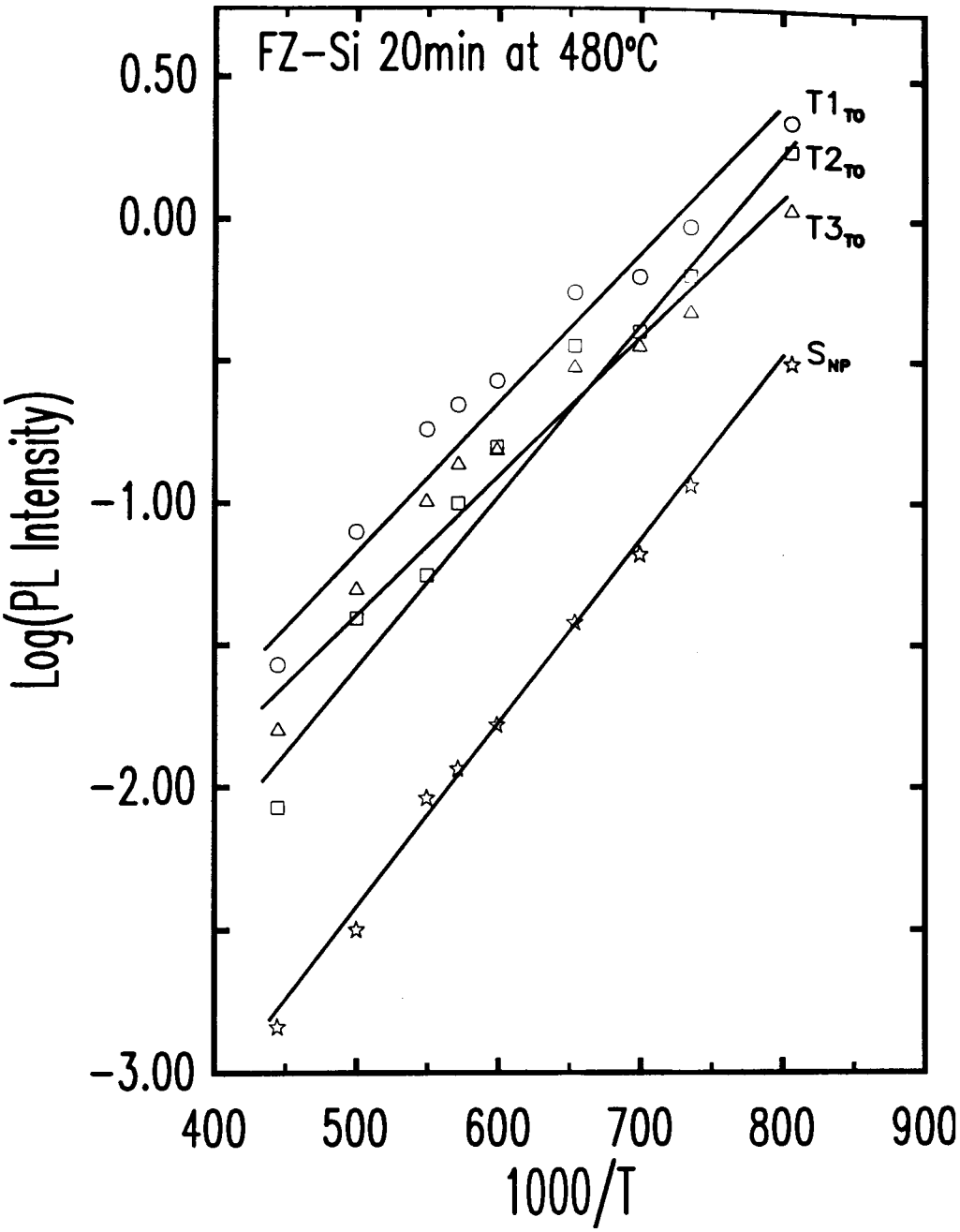

Figure 4.4 Plot of log PL intensities of the four lines, S_{NP}, $T1_{TO}$, $T2_{TO}$ and $T3_{TO}$ shown on Figure 4.3(c), versus inverse temperature. BE binding energies were measured from the slopes. For S_{NP}, $T1_{TO}$, $T2_{TO}$, and $T3_{TO}$ related TD BEs, their binding energy are 0.50, 0.38, 0.46 and 0.36 meV, respectively.

Furthermore, the lifetimes of the four transitions have been measured by collecting a histogram of PL intensity as a function of delay time following the exciting laser pulse, and making an exponential fit to the decay curve. The lifetime of S_{NP} line is 181 ns, while the lifetimes of the triplets $T1_{TO}$, $T2_{TO}$ and $T3_{TO}$ are 175, 181 and 193 ns, respectively. To check the system error of our lifetime measurements, the lifetime of B_{NP} of the quenched sample at 1.24K was measured. The lifetime of B_{NP} was 988 ns, which is quite close to the generally accepted 1055 ns. The lifetimes of S_{NP}, $T1_{TO}$, $T2_{TO}$ and $T3_{TO}$ are equal within our measurement error.

The four decays, S, T1, T2 and T3, have the same lifetime, and are due to the bound excitons having the same binding energy. We conclude that the four transitions are from the same initial exciton states localized on the same TD species. We call this TD species TDx, where x is the numbering of TD species as deduced from IR-absorption spectroscopy. Then S is the TDx bound exciton ground state to TDx ground state transition, while the triplet T1, T2, and T3 are the TDx BE ground state to TDx valley orbit excited state transitions. The S_{NP} line is separated from the triplet $T1_{NP}$, $T2_{NP}$ and $T3_{NP}$ by the energy of valley orbit splitting (VOS) which is around 188 cm^{-1} or 23.3 meV. By comparing this value with those in Table 2.2, it is tentatively suggested that this thermal donor species is TD7 which has a VOS of 22.6 meV from the calculation.

When a neutral TD localizes an exciton, there are a total of three electrons in the ground state. According to the Shell model of Kirczenow [77K], two electrons can occupy the doubly degenerate Γ_1 electron shell, while the other electron must go into Γ_3 or Γ_5 1s-like states (which are four- and six-fold degenerate, respectively, counting spin) since these states are the next lowest in energy after the Γ_1 state. The hole goes into single particle states which belong to the Γ_8 quartet. We denote the electron configurations of TD BE ground-state as $\{2\Gamma_1, \Gamma_{3,5}; \Gamma_8\}$. An electron in any of the Γ_1, Γ_3 and Γ_5 states can recombine with the Γ_8 hole and emit a photon. The transitions from the same TD BE initial state have the same localization energy and radiative lifetime as detected using PL spectroscopy.

The three TDx VOS states we observed may be due to the splittings of the 1s $\{\Gamma_1, \Gamma_3\}$ and 1s $\{\Gamma_1, \Gamma_5\}$ states. The electron transitions of the TDx (i~7) bound excitons are shown schematically in Figure 4.5.

In addition, we also measured the peak intensities of the PL transitions, S, T1, T2 and T3, in the no-phonon and TO phonon-assisted region. We found that the TO:NP intensity ratio for the S transition was 8.5, while the TO:NP intensity ratios for T1, T2 and T3 transitions were around 0.7. AS pointed out above, S is the TDx BE ground state to TDx ground state transition, which is a $\Gamma_{3,5}$ electron recombining with a Γ_8 hole, leaving two electrons in the Γ_1

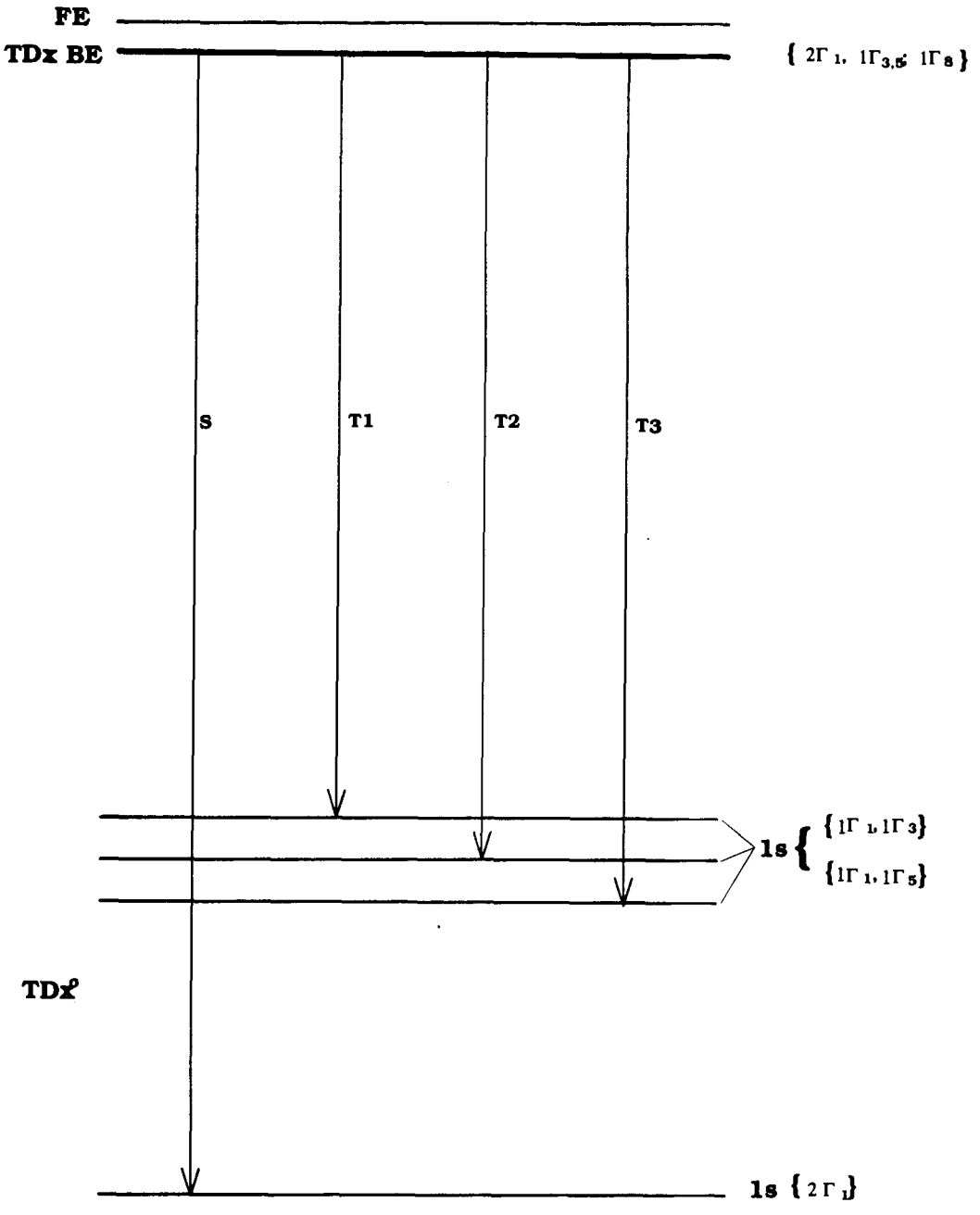

Figure 4.5 Electron transition schemes for TDx (x~7) bound excitons in case of the ground states of TDx BEs being {$2\Gamma_1$, $\Gamma_{3,5}$; Γ_8}.

electron state. T1, T2 and T3 are the TDx BE ground state to TDx valley-orbit excited state transitions, which is a Γ_1 electron recombining with a Γ_8 hole, leaving one electron in a Γ_1 electron state and another electron in a Γ_3 or Γ_5 electron state. In the TD BE complexes, electrons in the Γ_1 electron state have a much larger wave-function amplitude near the donor site (the central cell region) than that of electrons in the $\Gamma_{3,5}$ electron states. It is the scattering of an electron by the short-range impurity potential which leads to NP luminescence in the donor complexes. Although the holes are repelled by the positively charged ion core, electrons in the Γ_1 state have a high probability of being near the donor site and the no-phonon process is strong. Recombination of a Γ_8 hole with an electron in the $\Gamma_{3,5}$ states is more likely to involve momentum conserving phonons since the electron wave function vanishes in the region of the donor. As a result, we observed a much greater TO:NP intensity ratio for the S transition than for the T1, T2 and T3 transitions.

Because the PL intensity reflects the concentration of a given impurity species [87M], the relative luminescence intensities from excitons bound to different TD species can be used to detect the change in the relative concentration of these species with annealing time. Figure 4.6 depicts the dependence of photoluminescence intensity from thermal donor bound excitons in the no-phonon region on annealing time. Four samples annealed for different time intervals from 20

minutes to 4 hours at 480°C were measured. The quenched sample is also included for comparison. All the spectra were taken at 1.24K with a resolution of 0.5 cm^{-1} and normalized to equal phosphorus peak intensity. Separate lines are well resolved in the spectra, and the signal-to-noise ratio is high.

Figure 4.6 illustrates the drastic changes of the PL spectra from thermal donors upon annealing time. The relative concentrations of different TD species change most rapidly at the beginning of the annealing process. As annealing proceeds, the relative intensities of PL lines from the substitutional boron- and aluminum- related BEs to the substitutional phosphorus- related BEs decrease noticeably, which suggests that there is a considerable loss of B and Al from substitutional sites during annealing. The loss of substitutional Al during annealing was reported in [88D], and a decreasing of boron BE line intensity after annealing was also observed in [86W] and [88D]. However, as shown in the 4-hour sample PL spectrum, the total intensity of the TD-related lines is at least two orders of magnitude higher than the P BE line intensity, and from resistivity measurement, the total thermal donor concentration in this sample is well over 10^{15} cm^{-3}, while in our sample the P concentration is at the same level of Al concentration ($\sim 10^{12}$), and one order of magnitude lower than the boron

Figure 4.6 Annealing-time dependence of PL from TD BE in the NP region for a set of identical FZ-Si samples annealed in air at 480°C. The spectra have been normalized to equal P_{NP} height. PL spectra were recorded at 1.24K with a resolution of 0.06 meV. S_{NP} denotes the shallowest TD BE recombination, and Ti_{NP} (i=1,2,3) are its triplet. BD is a "boundary" that PL new lines appear and shift from both side toward and grow up upon annealing. BD is the separation between TD BE ground state to TD ground, and TD BE ground state to TD valley orbit excited state transitions.

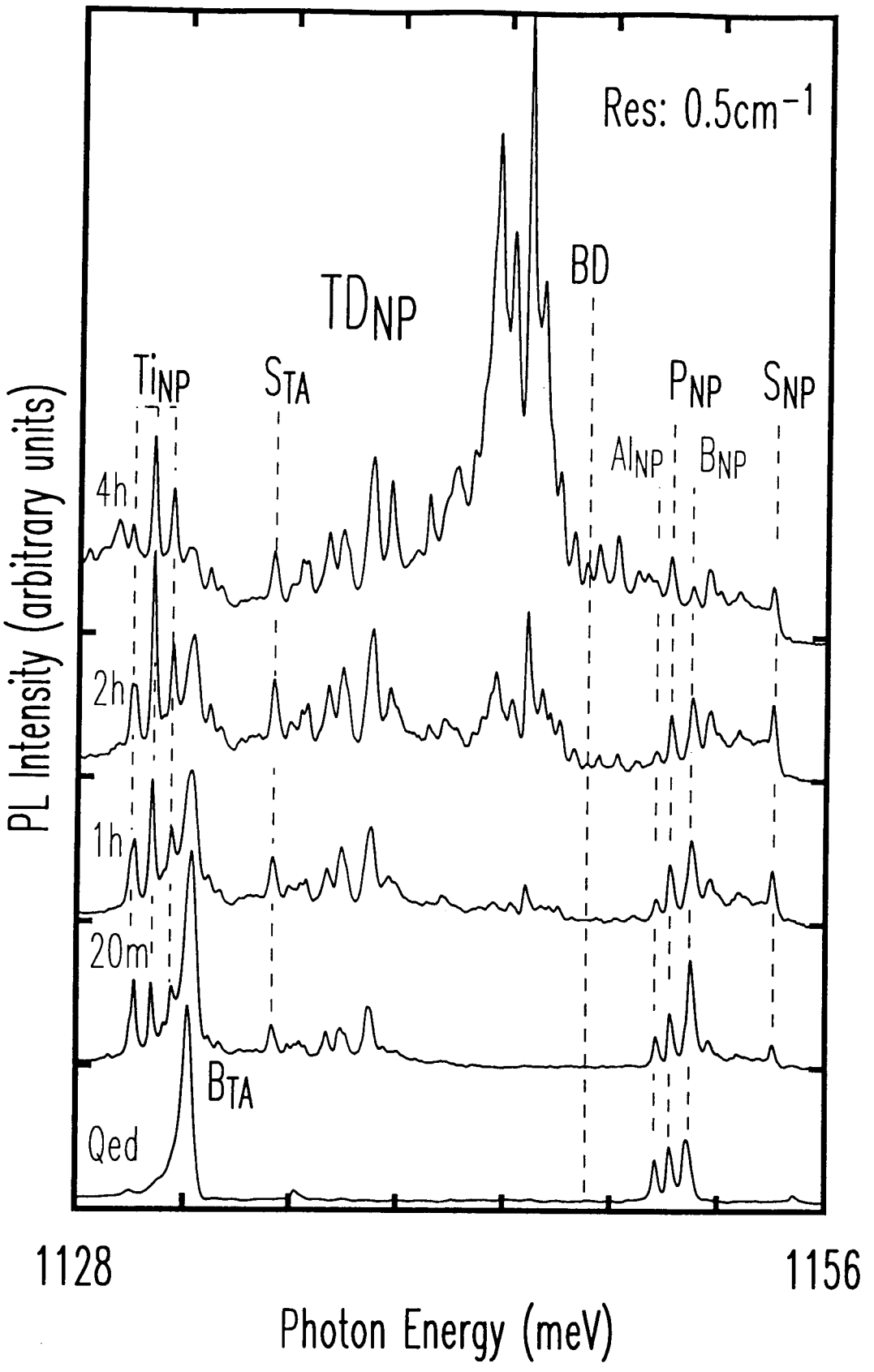
Res: 0.5cm^{-1}
TD$_{NP}$
BD
Ti$_{NP}$
S$_{TA}$
P$_{NP}$
S$_{NP}$
Al$_{NP}$
B$_{NP}$
4h
2h
1h
20m
B$_{TA}$
Qed
PL Intensity (arbitrary units)
1128
1156
Photon Energy (meV)

concentration (~10^{13}). The tiny amount of residual impurities in our samples rules out the possibility that the acceptor dopant in the starting material can play an important role in the formation of thermal donors. In addition, these data also confirm that these TD lines were directly associated with the thermal donors rather than due to BE recombination at boron-TD complexes. While some TD-associated BE PL lines arise after very short anneal times (20 minutes) in the two spectral regions from 1129.9 to 1139.9 meV and from 1150.7 to 1154.2 meV, their relative intensities do not significantly change with longer annealing. With prolonged annealing, new luminescence lines emerge in the region between 1139.9 to 1149.6 meV and become the dominant feature. However, for the 1-hour to 4-hour samples, the same TD species can be accounted for in this NP region, although the intensities of the PL lines change upon annealing time.

Figure 4.6 can also be analyzed in another way. We can separate the spectra into two regions, the higher energy side and the lower energy side, by a "boundary"--line BD. When the annealing time increases, new peaks appear from the far side in both regions and approach closer to BD. Some of these new peaks grow so quickly that they soon become the dominant features of the spectrum. Eventually, the left and right spectral regions merge and the "boundary" disappears as seen in the 2-h and 4-h annealed sample spectra. There are more than 40 separate and reproducible lines in the 2-h and 4-h sample spectra, while there are only ten or so

identified TD species [83P, 89W, 92G]. In Figure 4.6, there are about 11 TD-related PL lines in the higher energy side, and about 33 TD-related PL lines in the lower energy side.

The explanation for the "boundary" BD, and the large number of PL lines is that the lines on the higher energy side are the TD bound exciton ground state to TD ground state transitions, while the more complicated lines on the lower energy side are the TD bound exciton ground state to TD valley orbit excited state transitions. In fact, S_{NP} denotes the observed shallowest TD BE ground state to TD ground state transition, and Ti_{NP} (i=1,2,3) denotes the observed shallowest TD BE ground state to TD valley orbit excited state transitions, while the "BD" line, which is around the energy position of 1146.45 meV, corresponds to the deepest thermal donor bound exciton recombination. The bound exciton binding energy of the deepest thermal donor species is around 8.04 meV which is the energy difference between the "BD" line and the FE_{NP} edge.

We observed that later TD species form deeper bound excitons and have smaller valley orbit splittings than those of the earlier TD species. The very late thermal donor species have valley orbit splittings, which are the splittings between the TD 1s $\{2\Gamma_1\}$ and 1s $\{1\Gamma_1, 1\Gamma_3\}$ ($\{1\Gamma_1, 1\Gamma_5\}$) states, smaller than 1 meV.

However, except for TDx (x~7), we are unable to conclusively identify from thermalization and PL lifetime measurements the transitions of certain thermal donor

species from the BE ground state to the TD ground state and from the TD BE ground state to the TD valley orbit state. This is due to the relatively weak PL lines from the TD BE ground state to TD ground state transitions, and the many different TD species and the small differences among them. The lifetime differences and the thermalization effects are not sufficiently obvious in the PL spectra.

As mentioned before, the shallowest TD BEs observed at 1.24K are most probably TD7 BEs. The deepest TD BEs may be TD18, as 11 TD BE ground state to TD ground state transitions have been observed. This seems to contradict the existence of only ten TD species, as is generally accepted. In fact, no one knows the actual number of thermal donor species. From IR-absorption spectroscopy studies, TD1 to TD9 are reported in [83P], TD1 to TD11 in [89W], and TD12 to TD16 in [92G]. If the actual binding energy of TD 1s $\{1\Gamma_1$, $1\Gamma_3\}(\{1\Gamma_1$, $1\Gamma_5\})$ is greater than the one used (the binding energy of phosphorus 1s $\{\Gamma_3\})$, the VOS will shift toward lower energy from the calculated ones, and the identified TD species may turn out to be TDn with n less than 7. This is quite probable, noting that TDs are He-like effective mass double donors with ground state binding energies of around 60 meV, while phosphorus is a H-like single donor with a ground state binding energy of 45.5 meV [65A]. The deepest TD BE becomes TDn BE with n less than 17, which is consistent with the total TD species observed in IR-absorption studies [92G].

As previously mentioned, the peak intensity ratio of the strongest lines in the TD_{TO} and TD_{NP} band of the PL spectra from the 4-hour annealed sample is about 7. These lines result from recombination of a Γ_8 hole and a Γ_1 electron in excitons bound at very late TD species (TDn with n probably larger than 12). The TO:NP intensity ratios for T1, T2 and T3 transitions, which also are recombination of a Γ_8 hole with a Γ_1 electron in excitons bound at an "early" TD species (TDn with n~7), are 0.7. It appears that when the number n increases, the TO:NP intensity ratio for the BE at TDn species increases rapidly, which implies either that the TDn BE electrons in the Γ_1 state have a decreasing wave function amplitude in the central cell region or that the central cell potential is decreasing. It was suggested that the very large TO:NP intensity ratio for the BEs indicates binding to a center with an extended strain-well potential [89S]. We conclude that the strain-well potential of TDn extends as the number n of the TDn species increases, despite the fact that the TD ionization energy decreases with the TD species number n. This is perhaps evidence of growing clusters of thermal donors.

Heijmink Liesert et al. [92H, 93H] reported that the TD_{TO} band shifts toward higher photon energy upon annealing, with a simultaneous change of its total intensity. In fact, their TD_{TO} band is just the TO phonon-assisted TD BE ground state to TD valley orbit excited state transitions, which shift toward higher photon energies upon heat treatment. The

TD bound exciton ground state to TD ground state transitions, which are much weaker than the TD BE ground state to TD valley orbit state transitions, shift toward lower photon energies upon heat treatment. Their conclusion that the exciton localization energy becomes consequently smaller upon heat treatment is obviously wrong because they have mistaken the TD BE ground state to TD valley orbit excited state transitions as being due to the TD BE ground state to TD ground state transitions.

It is generally accepted that successively shallower species of thermal donors are sequentially introduced upon annealing. Their first ionization energies range from 69.3 to 53 meV [83P]. From Haynes' Rule, $E_{BX}=a+bE_i$ (Equation 1.3) where the values a and b for normal shallow donor and acceptor impurities in Si were observed to be approximately 0 and 0.1, respectively [60H], the exciton binding energy E_{BX} is predicted to be about a tenth of the impurity ionization energy E_i in Si. It is normally expected that the shallower the donors, or the smaller the donor ionization energies, the smaller the binding energies of their bound excitons. However, from Figure 4.5, this is not true for the thermal donor system in silicon. The TD bound exciton binding energy ranges from 0.50 to 8.04 meV. In fact, for the earlier time, or deeper, thermal donor species, their bound exciton binding energies become smaller. For the TD system in silicon the factor "a" must be positive and "b" must be negative if the Haynes' Rule $E_{BX}=a+bE_i$ is still

tenable. Therefore, Haynes' Rule with a~0 and b~0.1 is not valid for the thermal donor system in silicon. Since we cannot obtain with certainty both the TD ionization energy and the TD bound exciton binding energy for specific TD species, we do not know whether Haynes' Rule still holds or not, and thus it is not reasonable for us to assign any values to the factors a and b at this time.

Chapter Five
Conclusions

This work is the first detailed and complete photoluminescence study of thermal donors in silicon. State-of-the-art high-resolution PL spectra with very good signal-to-noise ratio have been obtained. The dependence of the thermal donor bound exciton related PL intensities on both annealing time and measurement temperature has been investigated.

More than 40 PL transitions of thermal donor bound excitons were clearly resolved at the temperatures as low as 1.24 Kelvin, which directly confirms the multispecies character of thermal donors. It was found that both thermal donor ground states and valley orbit excited states play significant roles in TD luminescence. Among the over 40 transitions observed, we identified, for the first time, four which: a) are due to the recombination of bound excitons with the same binding energy and b) have the same lifetime. This indicates that the four transitions are from the same initial exciton states localized on the same thermal donor species. It is also the first time that the measurement of valley-orbit splitting for this thermal donor species has been accomplished. This TD species has also been correlated with a thermal donor species studied using

infrared absorption spectroscopy by comparing the valley-orbit splitting.

It was found that the TO:NP intensity ratio for the TD bound exciton ground state to the TD valley-orbit excited state transitions increased rapidly with the TD species numbering. This means that the strain-well potential of thermal donors extends with the TD species numbering. This evidence favors a growing cluster model for TD formation.

The exciton binding energies of thermal donors have been found to range from 0.50 to 8.04 meV, which is much smaller than the values reported by other studies. The early-time thermal donor BE binding energies were found to be very small ($\leq$ 0.5 meV). Some very early thermal donor species may not be able to localize free excitons even at very low temperature (~0.5K).

The earlier a thermal donor species is introduced into the silicon crystal during thermal annealing, the deeper its donor ground state is, while the shallower its bound exciton becomes. Therefore, the normally accepted Haynes' rule $E_{BX}=a+bE_i$ with the factors a~0 and b~0.1 for silicon is invalid for the thermal donor system in silicon.

The later time TD species have smaller valley orbit splittings than those of the earlier ones. The valley orbit splitting of the latest TD species is very small, less than 1.0 meV, compared to the valley orbit splittings of around 24 meV for the early thermal donor species.

REFERENCES

37W G.H. Wannier, Phys. Rev. 52, 191 (1937).

54F C.S. Fuller, J.W. Dietzenberger, N.B.Hannay, and E. Buehler, Phy. Rev. 96, 833 (1954).

55K W. Kohn and J.M.Luttinger, Phys. Rev. 98, 915 (1955).

57F C.S. Fuller and R.A.Logan, J. Appl. Phys. 28, 1427 (1957).

57K W. Kaiser, Phys. Rev. 105, 1751 (1957).

58H H.J. Hrostowsky and R.H.Kaiser, Phys. Rev. Lett. 1, 199 (1958).

58K W. Kaiser, H.L.Frisch, and H.Reiss, Phys. Rev. 112, 1646 (1968).

58L M.A. Lampert, Phys. Rev. Lett. 1, 450 (1958).

60H J.R. Haynes, Phys. Rev. Lett. 4, 361 (1960).

63K K.Nishikawa and R.Barrie, Can. J. Phys. 41, 1135 (1963).

65N R.C. Newman and J.B. Willis, J. Phys. Chem. Solids, 26, 373 (1965).

67D P.J.Dean, J.R.Haynes, and W.F.Flood, Phys. Rev. 161, 711 (1967).

70K A.S.Kaminskii and Ya.E.Pokrovskii, Pis'ma Zh ETF 11, 381 (1970). [Engl. Transl. JETP Lett. 11, 255 (1970)].

72B A.R.Bean and R.C.Newman, J. Phys. Chem. Sol. 33, 255(1972)

73D P.J. Dean, *Luminescence of Crystals, Molecules, and Solutions*, ed. by F.E. Williams (Plenum Press, New York, 1973), p538.

73S R.Sauer, Phys. Rev. Lett. 31, 376 (1973).

74K K.Kosai and M.Gershenzon, Phys. Rev. B9, 723 (1974).

75B F.Bassani and Pastori Parravicini, *Electronic States and Optical Transitions in Solids* (Oxford Pergamon, 1975).

75G K.Graf and H.Pieper, J.Electron. Mater. 4, 281 (1975).

76B A.Baldereschi, and N.O. Lipari, *Proceeding of Thirteenth International Conference on the Physics of Semiconductors*, (Rome, 1976), p595.

76D P.J.Dean, D.C.Herbert, D.Bimberg, and W.J.Choyke, Phys. Rev. Lett. **37**, 1635 (1976).

76M T.N. Morgan, Proceedings of Thirteenth International Conference on the Physics of Semiconductors, (Rome, 1976), p825.

76S R.Sauer, Journal of Luminescence **12/13**, 495 (1976)

77H O.Helmreich and E.Sirtl, in Semiconductor Silicon 1977, ed. by R.H.Huff and E.Sirtl, (The Electrochemical Society, Princeton, 1977), p626.

77K G.Kirczenow, Solid State Comm. **21**, 713 (1977).

77R T.M.Rice in Solid State Physics, Vol.32, ed. by H.Ehrenreich, F.Seitz, and D.Turnbull, (Academic Press Inc., New York, 1977).

77T$_1$ M.L.W.Thewalt, Can. J. Phys. **55**, 1463 (1977).

77T$_2$ M.L.W.Thewalt, Phys. Rev. Lett. 38, 521 (1977).

78M S.Muller, M.Sprenger, E.G.Sieverts, C.A.J.Ammerlaan: Solid State Commun **25**, 987 (1978)

78T M.Tajima, Appl. Phys. Lett. **32**, 719 (1978).

79D P.J. Dean and D.C. Herbert, in *Topics in current Physics* **14**, ed. by K. Cho (Springer, Berlin, Heidelberg, 1979).

79G P.Gaworewski and K.Shmalz, Phys. Stat. Sol. **A55**, 699(1979)

79T M.Tajima, A.Kanamori, and T.Iizuka, Jap. J. Appl. Phys. **18**, p.1401 (1979).

79W D.Wruck, P.Gaworzewski, Phys. Status Solidi (a) **56**, 557, (1979)

80M A.E.Mayer and E.C.Lightowlers, J. Phys. **C12**, L747 (1980).

80T$_1$ M.Tajima, S.Kishino, A.Kanamori, and T.Iizuka, J. Appl. Phys. **51**, 2247 (1980).

88T$_2$ M.Tajima, A.Kanamori, S.Kishino, and T.Iizuka, Jap. J. Appl. Phys. **19**, L755 (1980).

80T3 M.Tajima, J.Appl. Phys. 51, 2247 (1980).

81K L.C.Kimerling and J.L.Benton, Appl. Phys. Lett.39, 410, (1981).

81L M.Lannoo and J.Bourgin, *Point Defects in Semiconductors I, Theoretical Aspects*, Springer Series in Solid State Sciences, Vol.20, (Springer-Verlag, Berlin, 1981).

81N H.Nakayama, T.Nishino, and Y.Hamakawa, Appl. Phys. Lett. 38, 623, (1981).

81R A.K.Ramdas and S.Rodriguez, Rep. Prog. Phys. 44, 1297, (1981).

81S H.F.Schaake, S.C.Barber, and R.F.Pinizotto, in *Semiconductor Silicon 1981*, ed. by H.R.Huff, R.J.Kriegler, Y.Takeishi (The Electrochemical Soc., Inc., Pennington, N.J. 1981)

81T W.R.Turber, R.L.Mattis, Y.M.Liu, and J.J.Filliben, *The Relationship Between Resistivity and Dopant Density for Phosphorus-and Boron-doped Silicon*, (U.S. Government Printing Office, Washington 1981).

82K A.S.Kaminskii, L.I.Kolesnik, B.M.Leiferou and Ya.E.Pokrovskii, J. Appl. Spect. 36, 516 (1982).

82S K.Seeger, *Semiconductor Physics, An Introduction*, Springer Series in Solid State Sciences, Vol.40, (Springer-Verlag, Berlin, 1982).

82T M.L.W.Thewalt in *Excitons*, ed. by E.I.Rashba and M.D.Sturge (North Holand, New York) 394, (1982).

83O R.Oeder and P.Wagner, in *Defects in Semiconductor II*, ed. by S.Mahajan and J.W.Corbett (North Holland, New York, 1983), p.14.

83P B.Pajot, H.Compain, J.Lerouille and B.Clerjand, Physica 117B, 110, (1983).

83S M.Stavola, J.R.Patel, L.C.Kimmerling, and P.E.Freeland, Appl. Phys. Lett. 42, 73 (1983).

84W K.Wada, Phys. Rev. B 30, 5884, (1984).

85B A.Bourret, in *Proceedings of the XIII International Conference on Defects in Semiconductors*, ed. by L.C. Kimerling and J.M.Parsey, Jr. (TMS-AIME, New York, 1985), p.129.

85N R.C.Newman, J. Phys. C. 18, L967 (1985).

85S M.Stavola, K.M.Lee, J.C.Nabity, P.E.Freeland, and L.C. Kimerling: Phys. Rev. Lett. **54**, 2639, (1985).

86G P.R.Griffiths and J.A.de Haseth, *Fourier Transform Infrared Spectrometry*, (John Wiley an Sons, New York, 1986).

86M J.Michel, J.R.Niklas, J.M.Spaeth, and C.M.Weinert, Phys. Rev. Lett. **57**, 611 (1986)

86Sa M.Stavola, K.M.Lee: in *Oxygen, Carbon, Hydrogen, and Nitrogen in Silicon*, ed. by J.C.Mikkelsen, Jr., S.J.Pearton, J.W.Corbett, S.J.Pennycook, Symposia Proceedings, Vol. 59 (Material Research Society, Pittsburgh, Pa. 1986), p.95.

86Sb T.Steiner, Ph.D. Thesis, Simon Fraser University (1986).

86W P.Wagner: In Ref. [86sa] p125.

87G T.Gregorkiewicz, D.A.van Wezep, H.H.P.Th. Bekman, and C.A.J.Ammerlaan, Phys. Rev. **B35**, 3810, (1987).

87M P.McL Colley and E.C. Lightowers, Semicond. Sci. Tech. **2**, 157 (1987).

88B H.H.P. Th. Bekman, T. Gregorkiewicz, and C.A.J. Ammerlaan, Phys. Rev. Lett. **61**, 227 (1988).

88D A.C.T.Drakeford and E.C.Lightowlers: in *Defects in Electronic Materials*, ed. by M. Stavola, S.J.Pearton, G. Davies, Symposia Proceedings, Vol. 104 (Material Research Society, Pittsburgh, Pa. 1988) p209.

88M J.Michel, J.R.Niklas, and J.M.Spaeth: in Ref. [88D] p185

88Sa L.C.Snyder: in Ref.[88D] p.179.

88Sb A.G.Steele, Ph.D. Thesis, Simon Fraser University (1988).

89K Y.Kamiura, F.Hashimoto and M.Yoneta: *in Materials Science Forum* Vol. 38-41, (Trans Tech Publications, Switzerland, 1989) p.673

89L Landolt-BÖrnstein, *Numerical Data and Functional Relationships in Science and Technology, New Series*, group III, vol.22, Semiconductors, subvolume b, ed. by O.Madelung, (Springer-Verlag, Berlin 1989).

89S A.G.Steele and M.L.W.Thewalt, Can. J. Phys. **67**, p268 (1989).

89W P.Wagner and J.Hage, Appl. Phys. A **49**, 123 (1989).

92G W.GÖtz, G.Pensl, and W.Zulehner, Phys. Rev. B **46**, 4312, (1992).

92H B.J.Heijmink Liesert, T.Gregorkiewicz and C.A.J.Ammerlaan, Phys. Rev. B **46**, 2034 (1992).

92N M.K.Nissen, Ph.D. Thesis, Simon Fraser University (1992).

93H B.J.Heijmink Liesert, T.Gregorkiewicz and C.A.J.Ammerlaan, Phys. Rev. B **47**, 2034 (1993).

93L L.C.Lenchyshyn, Ph.D. Thesis, Simon Fraser University(1993).

94B H.Bender and J.Vanhellemont: in *Handbook on Semiconductors*, edited by S.Mahajan, (Elsevier Science BV, Amsterdam, 1994), vol. 3, pp1637-1753.